PETROPHYSICAL STUDY OF THE WEST EDMOND FIELD, IN PARTS OF OKLAHOMA, CANADIAN, KINGFISHER, AND LOGAN COUNTIES, OKLAHOMA

By

BRAYDN JOHNSON

Bachelor of Science in Geology

Texas Christian University

Fort Worth, Texas

2007

Submitted to the Faculty of the
Graduate College of the
Oklahoma State University
in partial fulfillment of
the requirements for
the degree of
MASTER OF SCIENCE
May, 2009

PETROPHYSICAL STUDY OF THE WEST EDMOND FIELD, IN PARTS OF OKLAHOMA, CANADIAN, KINGFISHER, AND LOGAN COUNTIES, OKLAHOMA

Thesis Approved:

James Puckette

Thesis Adviser

Jay Gregg

Ibrahim Cemen

Gordon Emslie

Dean of the Graduate College

TABLE OF CONTENTS

LIST OF FIGURES

Figure Page

CHAPTER I

INTRODUCTION

Location

The West Edmond Field is an important oilfield located in central Oklahoma. Historically, the West Edmond Field was a source for oil during WWII and critical to the Allied victory. Specifically, the field is located in T. 12N., R.4W., T. 13N., R.4W., T.14N., R. 4W and 5W. and T.15N., R.4W and 5W., Oklahoma, Canadian, Logan, and Kingfisher counties. The West Edmond Field is geologically located on the eastern flank of the Anadarko Basin.

The Anadarko Basin and central Oklahoma areas cover approximately 28,400 square miles. The basin contains in excess of 40,000 ft. of Paleozoic sediments near the axis (Adler, 1971; Hill, 1984). The Anadarko Basin is an asymmetrical west-northwest-east-southeast-trending remnant of the Southern Oklahoma Aulacogen (Hoffman, 1974; Kopaska-Merkel, 1989). The northern margin grades into the shallow dipping Anadarko Shelf near the Oklahoma Kansas border. The southern margin is defined by the Amarillo Mountains (Ham, 1964; Kopaska-Merkl, 1989). The Nemaha Ridge bounds the Anadarko Basin to the east. The western border is the Hugoton-Panhandle field (Hill, 1984). Figure 1 shows the geographic and geologic location of the West Edmond Field and its relationships to the tectonic provinces of Oklahoma.

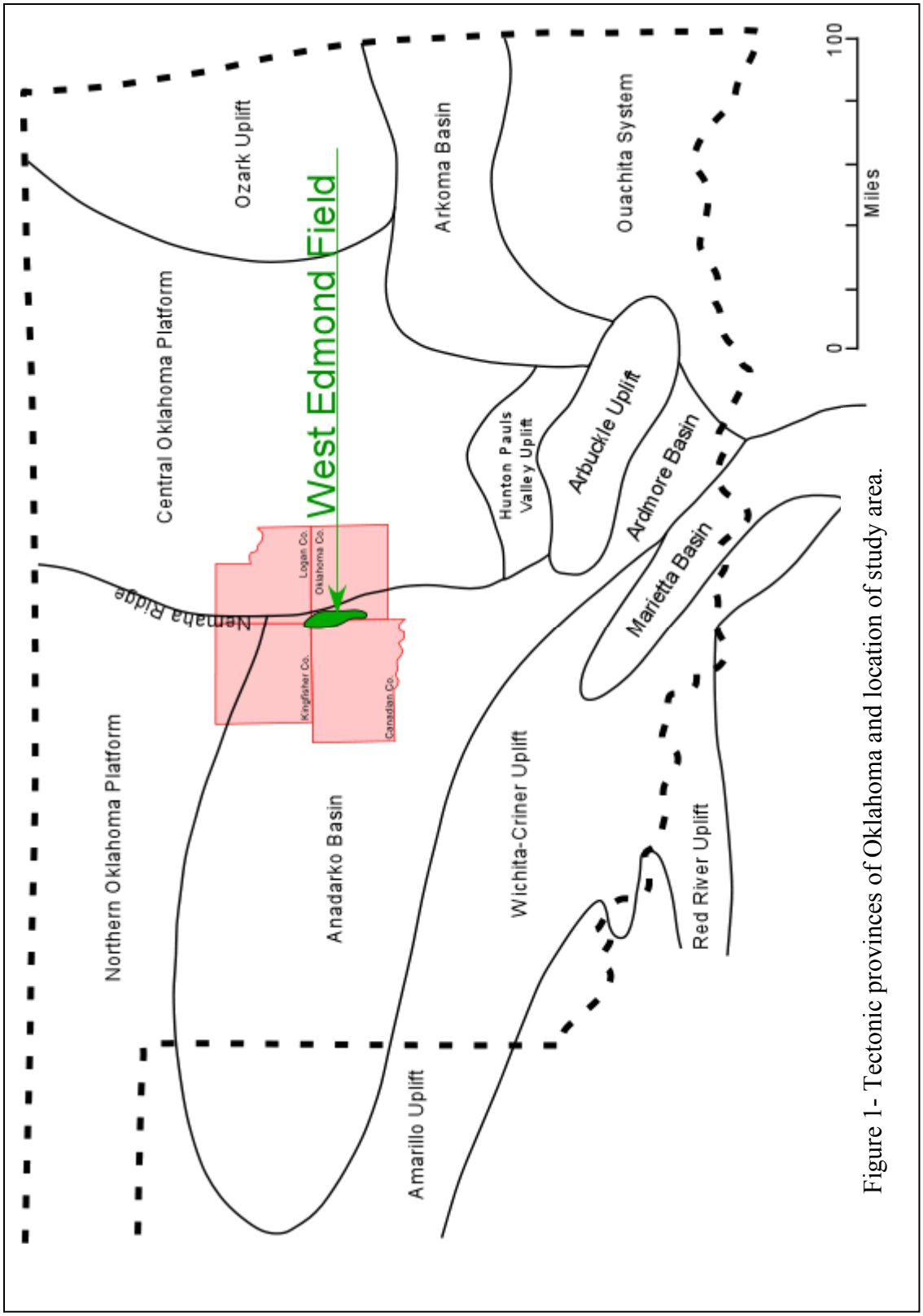

Figure 1- Tectonic provinces of Oklahoma and location of study area.

Purpose and Objectives

The West Edmond Field has produced 170,831,295 barrels of oil and 395,474,634 mcf of gas since its discovery (PI Dwights, 2008). Presently, the West Edmond Field is being redeveloped to recover remaining reserves of oil and gas. The pressing geologic questions concerning redevelopment include: 1) What depositional model explains the Hunton carbonates, and 2) Which depositional facies have better potential of producing additional volumes of oil and gas? It is proposed that the Hunton carbonates in the West Edmond Field represent shallow ramp deposits and carbonate mounds. Further, it is proposed that dolomitic mud rocks contain the bulk of the bypassed oil and gas remaining in the Hunton reservoir.

The purpose of this study is to evaluate the rock properties and reservoir facies of the Hunton Group carbonates, and determine their reservoir potential. The findings of this study will effect the redevelopment of mature carbonate fields. Core-derived porosity and permeability, and reservoir engineering data from studies in the 1940's, 1950's, and 1960's are not sufficient for the redevelopment of the West Edmond Field. To achieve the primary purpose and help interpret the prospects for redevelopment the following objectives were proposed:

1. Reconstruct the stratigraphy of the West Edmond Field using modern wire-line logs and recent advances in interpretations.

2. Establish a depositional model and sequences for the upper part of Hunton Group in the West Edmond Field.
3. Examine previous reservoir engineering studies of the West Edmond Field to establish pathways of fluid migration and reservoir characteristics.
4. Reaffirm and establish dominant porosity types within the upper Hunton Group using whole core analysis, thin sections, or scanning electron microscope images.
5. Construct petrophysical facies by integrating lithologic, porosity, petrographic, and modern wire-line log data.

Methods of Investigation

Multiple phases of data collection were employed to complete the objectives of this study. The first phase was a literature review of the stratigraphy of the Hunton Group.

The second phase of the research was the examination of depositional models of the Hunton Group and establishing a depositional model and sequences for the upper Hunton strata package in the West Edmond Field. One whole core from Chesapeake Energy, the West Edmond SWD # 1-24 well and 95 associated thin sections taken from

the core were scrutinized to help establish a depositional facies, and construct a depositional model for the upper Hunton carbonates.

The third phase of the study was a literature review of reservoir engineering studies of the West Edmond Field to examine the success of primary and secondary recovery projects.

The fourth phase was the petrographic analysis of the West Edmond SWD 1-24 core, with an emphasis on thin section examination, and scanning electron microscopy to interpret the porosity types and geometry.

The fifth and final phase of the study was the integration of rock data with log curves of 19 modern wire-line logs to establish petrophysical facies that can be used to map flow units within the upper Hunton Group.

Previous Works

Several papers describing the geology and production history have been written since the discovery of the West Edmond Field in 1943. The West Edmond Field was the second largest field in Oklahoma and played a role in fueling the World War II war efforts. The importance of the West Edmond Field to the Oklahoma oil boom and World War II cannot be understated. Swesnik (1945) wrote the "Geology of the West Edmond Oil Field, Oklahoma, Logan, Canadian, and Kingfisher Counties, Oklahoma," which was the first overview of the geology of the West Edmond Field. McGee and Jenkins (1946)

published the "West Edmond Oil Field, Central Oklahoma," and discussed the development of the West Edmond Field up to the date of publication. Littlefield and others (1947) published "A Reservoir Study of the West Edmond Hunton Pool, Oklahoma," and was the first to discuss reservoir attributes of the West Edmond Field. Elkins (1969) composed "Internal Anatomy of a Tight, Fractured Hunton Lime Reservoir Revealed by Performance—West Edmond Field," and argued previous assumptions of the reservoir through analysis of pressure and production data. These four papers were the main studies of the West Edmond Field, and the only published papers written specifically about the field to date.

CHAPTER II

GEOLOGIC SETTING

Hunton Stratigraphy

The first use of the term Hunton was by Taff in his work on the geology of the Atoka Quadrangle and his type section in (Sec. 8, T.15., R.,8E.), near the abandoned town of Hunton (Taff, 1902). Reeds (1911) subdivided the Hunton into Chimneyhill Limestone and Henryhouse Shale, Haragan Shale and Bois d'Arc Limestone. Reeds (1926) added the Frisco Limestone (Swesnik, 1945). The stratigraphy of the Hunton in central Oklahoma was confused by early exploration geologists. Any porous member of the upper Hunton was called the "Bois d' Arc" Limestone and the lower zones were the Haragan/Henryhouse Limestone and Chimney Hill Limestone. The stratigraphy of the Hunton is more definitive and was established by later studies.

The Hunton Group in the West Edmond Field is composed of the Keel Formation, Cochrane Formation, Henryhouse Formation, Haragan-Bois d'Arc Formation , and Frisco Formation as seen in Figure 2 (Rottman, 2000). The Chimneyhill Subgroup is made up of the Keel Formation, Cochrane Formation, Clarita Formation as seen in Figure 2. The Hunton Limestone is Ordovician, Silurian, and Devonian in age (Rottman, 2000).

The Keel Formation is Upper Ordovician System, Ashgillian Series, and Hirnantian Stage (Rottman, 2000). The type locality of the Keel Formation is Upper

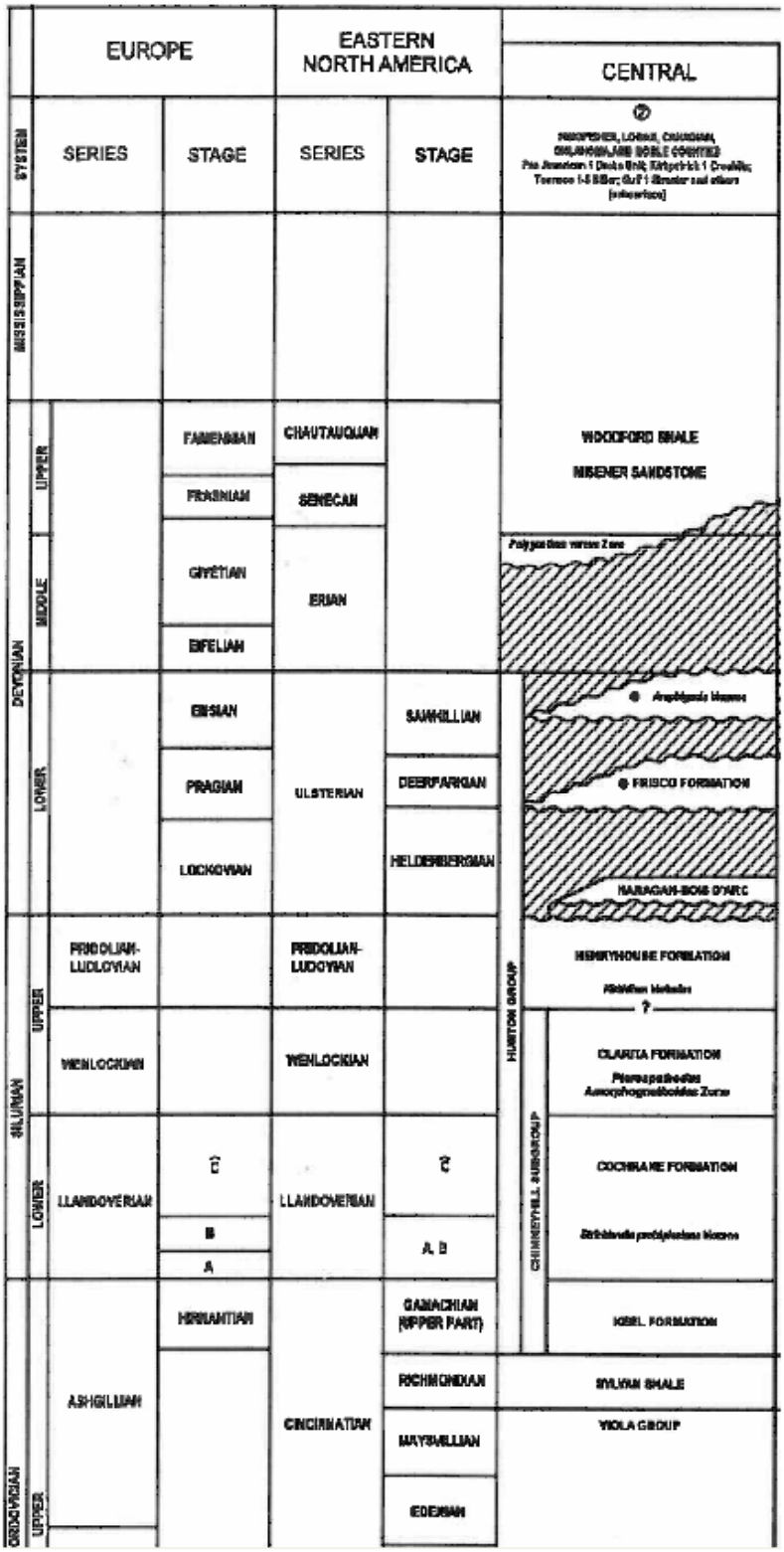

Figure 2. Stratigraphic nomenclature for the Woodford Shale, the Hunton Group, Slylvan Shale, and Viola Group in Central Oklahoma (Rottman, 2000).

Ordovician System, Ashgillian Series, and Hirnantian Stage (Rottman, 2000). The type locality of the Keel Formation is in Pontotoc County, Oklahoma (Amsden, 1960). The Cochrane Formation overlies the Keel Formation and is Lower Silurian System and Llandoverian Series (Rottman, 2000). The type locality for the Cochrane Formation is Pontotoc County, Oklahoma (Amsden, 1960). The Clarita Formation overlies the Cochrane Formation and is Upper Silurian and Wenlockian Series (Rottman, 2000). The type locality of the Clarita Formation is in Coal County, Oklahoma (Amsden, 1960). The Henryhouse Formation, which overlies the Clarita Formation, is Upper Silurian System and Pridolian-Ludlovian Series (Rottman, 2000). The type locality of the Henryhouse Formation is on Henryhouse Creek in Carter County, Oklahoma (Amsden, 1960). The Haragan-Bois d'Arc Formation, which overlies the Henryhouse Formation, is Lower Devonian System and Lockovian Stage (Rottman, 2000). The type locality of the Haragan-Bois d' Arc Formation is along Haragan Creek in Murray County, Oklahoma (Amsden, 1960). The Frisco Formation is unconformable to the Haragan-Bois d'Arc Formation or the older units it rests on (Rottman, 2000). The unconformity separating the Frisco Formation and pre-Frisco units can be the Silurian-Devonian boundary similar to that reported in Rechlin (2005). The unconformity represents the period of maximum erosion, truncation of the Hunton, and a time period of one to two million years (Fritz, 1994). The thinning of the Frisco Formation at the top of the Hunton is the result of pre-Woodford erosion (McGee, 1946). The Frisco Formation is Lower Devonian system Pragian Stage (Rottman, 2000). The type locality of the Frisco Formation is along Bois d'Arc Creek in Pontotoc County Oklahoma (Amsden, 1960, 1961). Figure 2 illustrates the stratigraphy of the Hunton Group in central and eastern Oklahoma.

Conodont Biostratigraphy

Conodont biostratigraphy was used to correlate wire-line log signatures of the Hunton group to stratigraphic boundaries (Rechlin, 2005). The wire-line logs of the West Edmond SWD 1-24 (Sec. 24, T.14N., R.5W.), Canadian County, Oklahoma, were correlated to the conodont biostratigraphic/petrophysical stratigraphic framework developed by Rechlin (2005). This wire-line log correlation was tied to the West Edmond SWD 1-24 core. A scour surface located at 7,110.8 ft. core depth, (Figure 3) is interpreted as the contact between Frisco Formation and pre-Frisco carbonates. The conodont species *Icrodius Claudia* and *Dvorkia* species are indicative of the Frisco Formation (Rechlin, 2005). A complete listing of the fauna present in the Hunton is included in the vast works of Thomas W. Amsden, (1958, 1960, 1961, 1962, 1967, 1975, 1980, and 1988). The contact between the pre-Frisco carbonates and the overlying Frisco Formation appears gradational on vintage wire-line logs with only spontaneous potential (SP) and resistivity curves, and is nearly impossible to separate (Swesnik, 1945). Figure 4 is a correlation of the West Edmond SWD 1-24 wire-line logs to the observed wireline-log response in (Rechlin, 2005) study area. The Frisco Formation is significantly thinner, but the pre-Frisco carbonates are appreciably thicker. The Clarita Formation is of analogous thickness between the two localities.

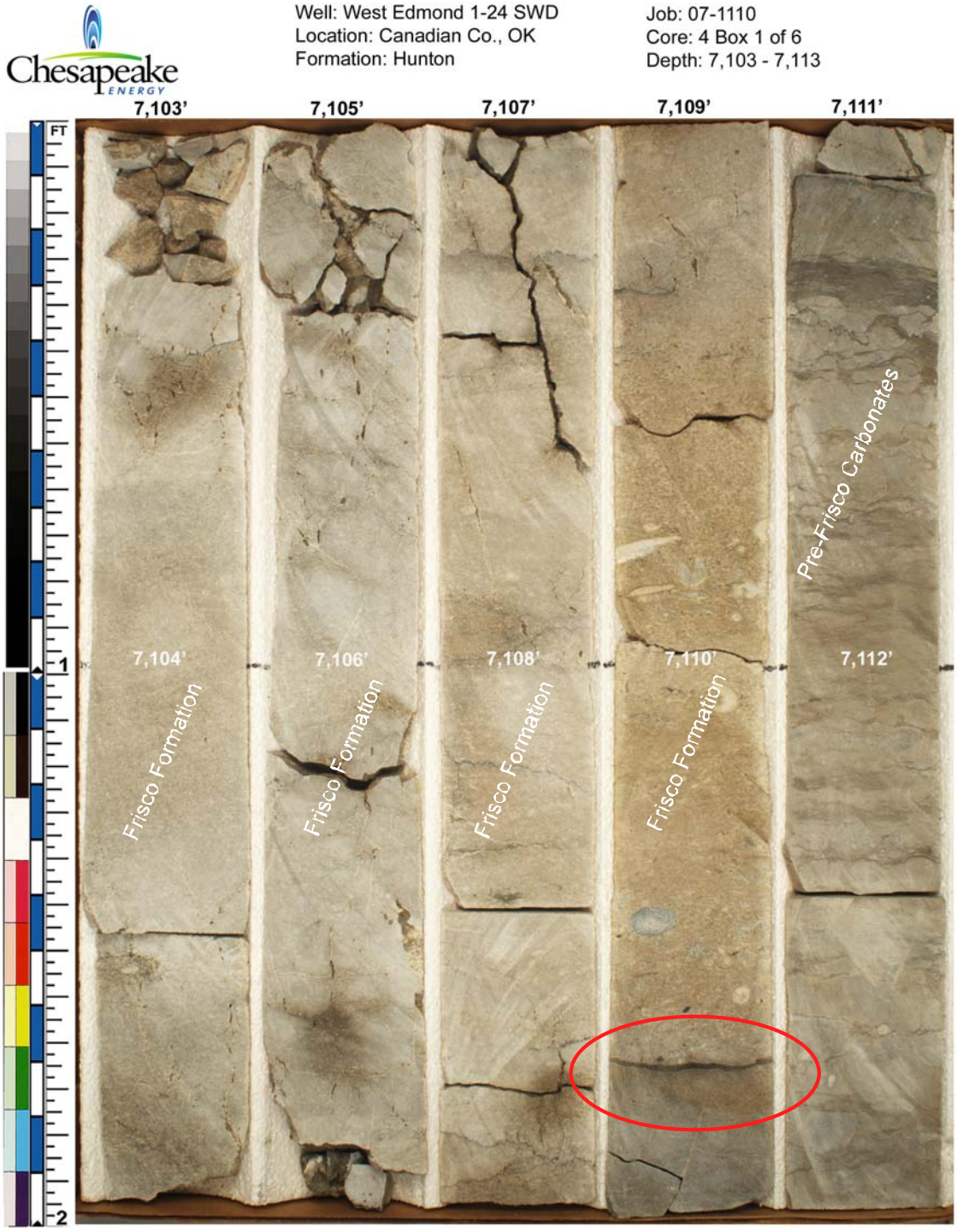

Figure 3. Proposed unconformity surface between the Frisco Formation and pre-Frisco carbonates.

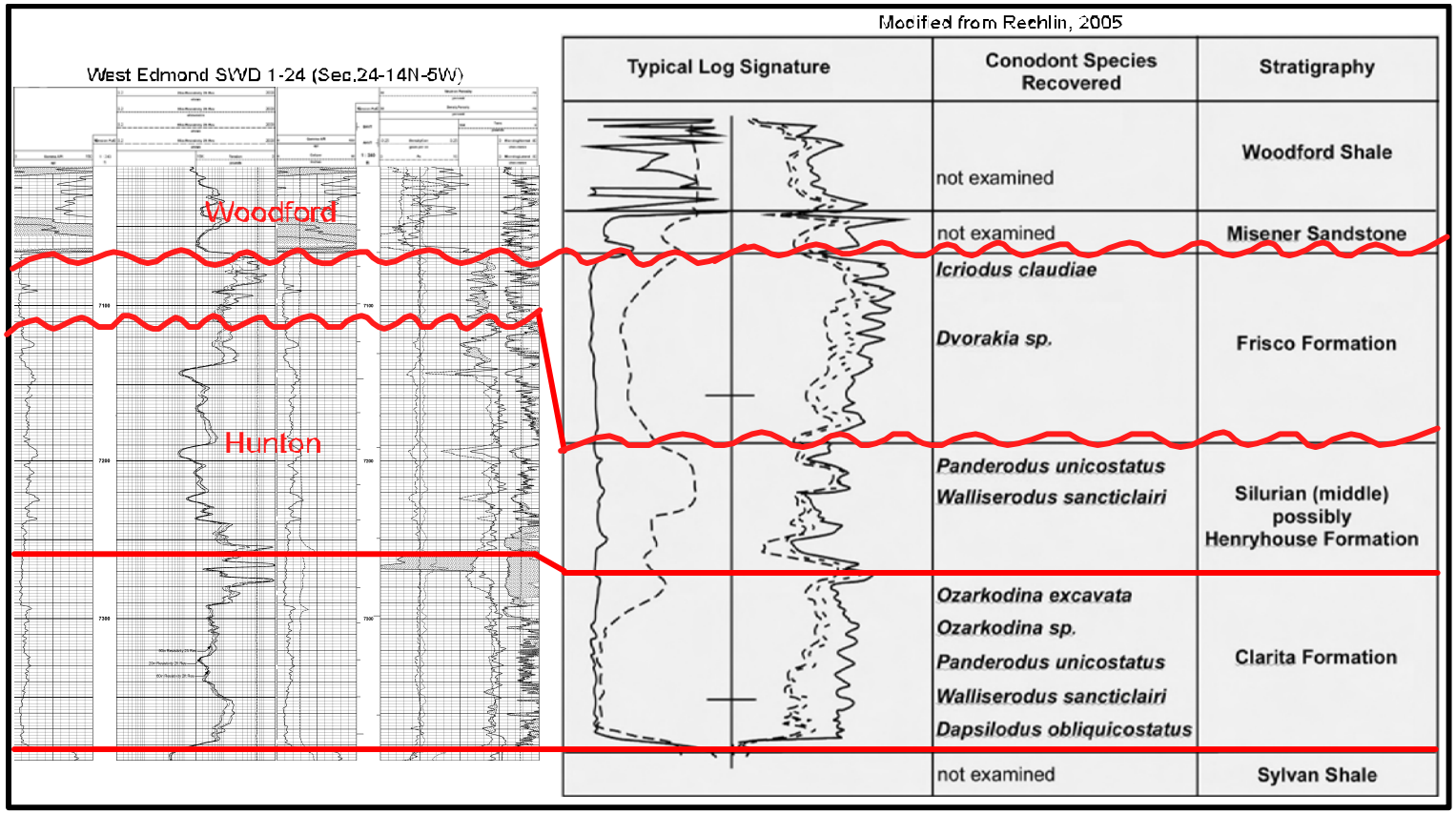

Figure 4. Correlation of wire-line logs from the West Edmond SWD 1-24 to wire-line log signatures and Hunton Group conodont biostratigraphy modified from Rechlin (2005).

Structure

The structural attitude of the West Edmond Field is a result of a local and regional tectonics. The Hunton Group is overlain by the relatively impermeable Woodford Shale (McGee, 1946). The regional structure of the West Edmond Field is a west dipping monocline (McGee,1946, Swesnik,1945). The tectonic environment during the Ordovician was quiescent. The Acadian orogeny was the first regional tectonic activity to disturb the Hunton Group. The Oklahoma City uplift began to rise in the Ordovician and continued to rise into the Permian (McGee, 1946). The uplift affected an area approximately 25 miles east to west and 40 miles north to south (McGee, 1946). The West Edmond field was relatively low structurally compared with the Oklahoma City anticline. Evidence indicates that in the hiatus between the Devonian and Mississippian, the north end of the field was higher structurally, and probably underwent more erosion and truncation than further south (McGee, 1946). A relict channel filled with Woodford Shale separates the field into a north half and south half and partitions the Frisco Formation. Figure 5 depicts the structure of top of the Hunton Group in the West Edmond Field.

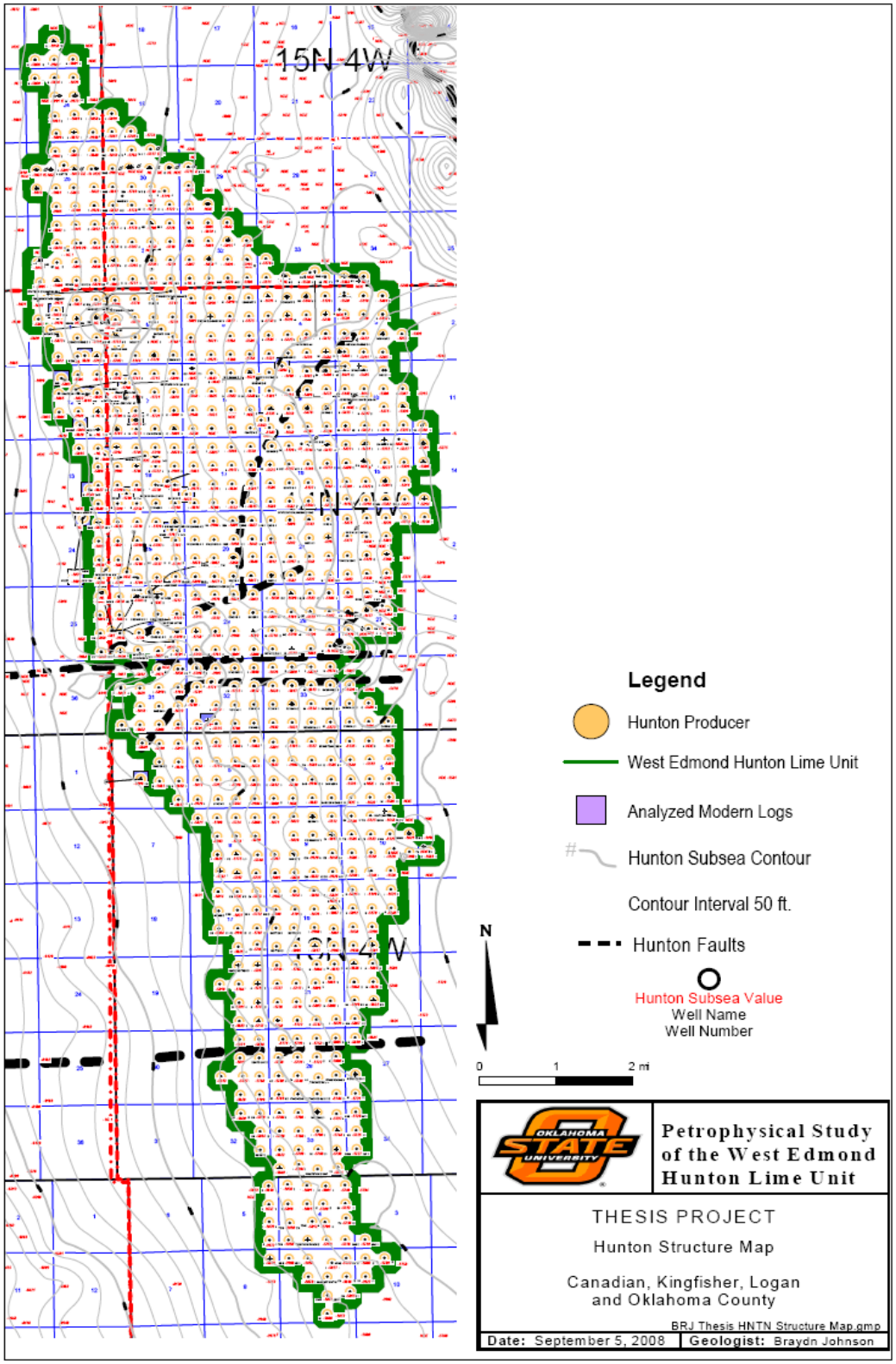

Figure 5. Structural map of the West Edmond Field contoured on the top of the Hunton Group. Countour interval is 25 ft. Outline of the "West Edmond Hunton Lime Unit" is shown in green.

CHAPTER III

DEPOSITIONAL ENVIRONMENT

Core Description

The West Edmond SWD 1-24 cored 83 feet of Hunton from 7,071.5 ft. to 7,155 ft., and the core description can be viewed in Figure 6. There was a total of 4 ft. of unrecovered Hunton between 7,083 ft. to 7,079 ft.

The calcareous muddy dolostone 7146-7147 ft. is top of what is interpreted as a shallowing upward sequence. The calcareous muddy dolostone may represent a sabkha type deposit. The dolomite within the calcareous muddy dolostone might be a function of diagenetic changes penecontemporaneous with deposition.

Mottled facies likely resulted from bioclastic material that was washed into an offshore or lagoonal environment dominated by lime mud accumulations. The mottled facies underwent differential compaction related to soft-sediment deformation, and/or bioturbation, which produced a pseudonodular fabric characteristic of deeper water facies. The mottled facies is locally oil-stained at the top, but more commonly lacks oil-stain due to reduced porosity and permeability. Wackestone is interpreted as evidence of sporadic quiescent subtidal conditions at the base of a shallowing-upward sequence.

Oil-stained oolitic facies is well sorted, wavy laminated to cross-bedded, grain supported limestone. The oolitic facies contains limestone rip-up clasts, pelmatazoan

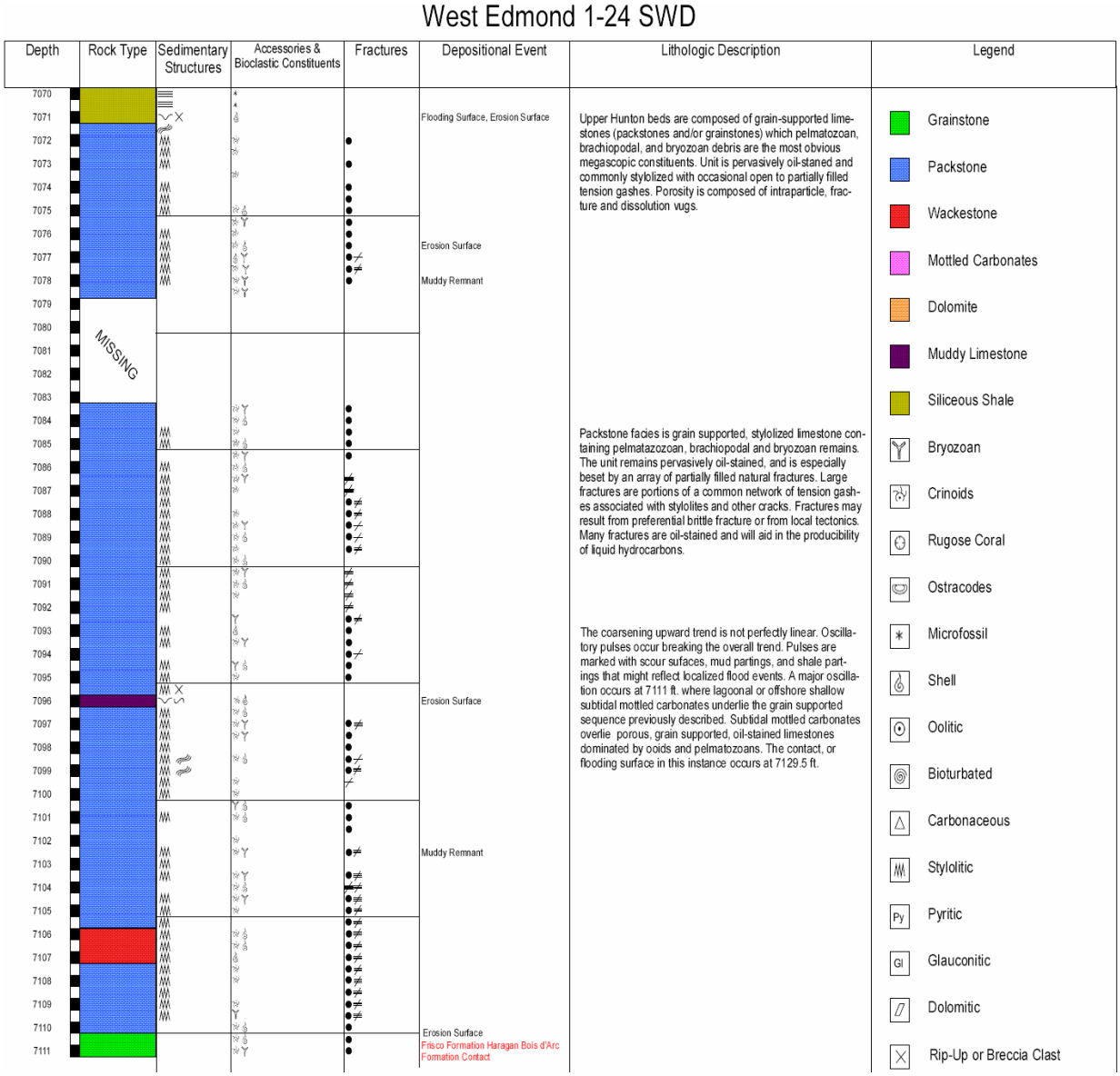

Figure 6. Core description of the West Edmond SWD 1-24.

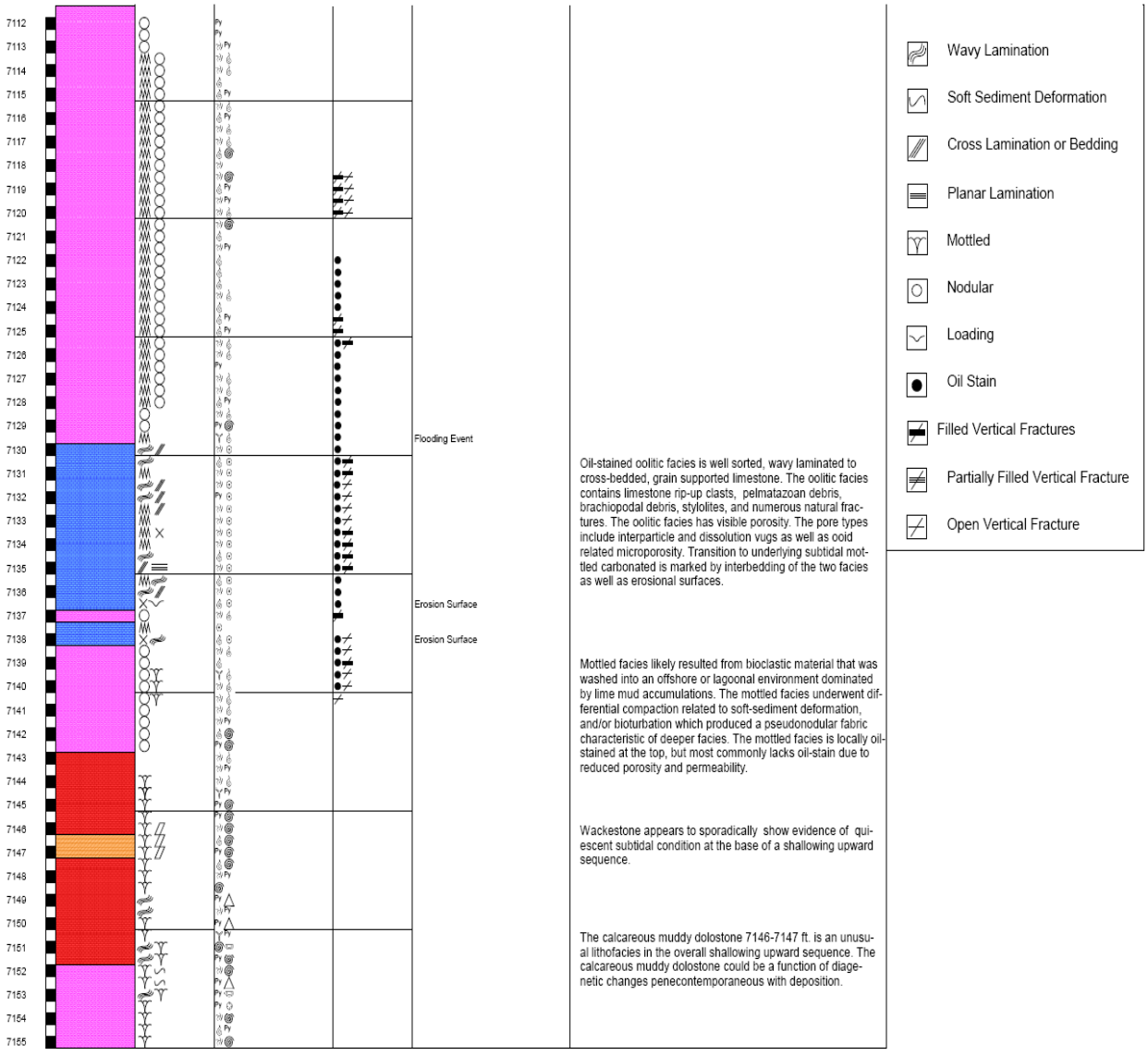

Figure 6. Core description of the West Edmond SWD 1-24 (Continued).

debris, brachiopodal debris, stylolites, and numerous natural fractures. The oolitic facies has visible porosity. The pore types include interparticle and dissolution vugs as well as ooid related microporosity. The transition to the underlying mottled carbonates is marked by interbedding of the two facies as well as erosional surfaces.

The coarsening-upward trend from mottled facies to the oolitic facies is not perfectly linear. Oscillatory pulses occur breaking the overall trend. Pulses are marked with scour surfaces, mud partings, and shale partings that might reflect localized flood events. A major oscillation occurs at 7,111 ft. where lagoonal or offshore shallow subtidal mottled carbonates overlie the packstone facies. Subtidal mottled carbonates overlie porous, grain supported, oil-stained limestones dominated by ooids and pelmatozoans. The contact, or flooding surface in this instance occurs at 7,129.5 ft.

Packstone facies is grain supported, stylolized limestone containing pelmatozoan, brachiopodal and bryozoan bioclasts. The unit is pervasively oil-stained, and is especially beset by an array of partially filled natural fractures. Large fractures are portions of a common network of fractures associated with stylolites and other cracks. Many fractures are oil-stained, indicating they are petroleum conduits.

Upper Hunton beds are composed of grain-supported limestones (packstones and/or grainstones) in which pelmatozoan, brachiopod, and bryozoan debris are the more obvious megascopic constituents. The unit is pervasively oil-stained and commonly stylolitized with occasional open to partially filled fractures. Porosity is composed of intraparticle, fracture, and dissolution vugs.

Depositional Environment Facies

The depositional facies of the Frisco Formation, and the pre-Frisco carbonates of the West Edmond field were classified using a similar system to the Hunton depositional system developed by Al-Shaieb (2000). The depositional model can be divided into three depositional facies that in turn can be further subdivided. Facies I through facies III are related to water depth. Facies I is the highest or shallowest water facies and facies III is the deepest water facies, which represents a subtidal to open marine setting.

Facies I sediments were deposited on the supratidal tidal flat near or above the mean high tide (Al-Shaieb, 2000) (Roehl, 1967). Facies I was deposited in a shallow restricted environment (Al-Shaieb, 2000). Facies I can be divided into two subfacies: karst/subaerial diagnenetic terrain and supratidal.

Facies II sediments were deposited in a shallow restricted subtidal to upper intertidal environment. Facies II is subdivided into lagoonal facies and oolitic shoal facies (Al-Shaieb, 2000).

Facies III sediments were deposited in a subtidal environment (Al-Shaieb, 2000). Facies III can be divided into four subfacies: bioherm/mound, upper subtidal, lower subtidal, and open marine. Facies and their subdivisions can be seen in Figure 7.

The open marine depositional environment falls at the base of facies III. The mudstone in the West Edmond SWD 1-24 core is a slightly dolomitized skeletal

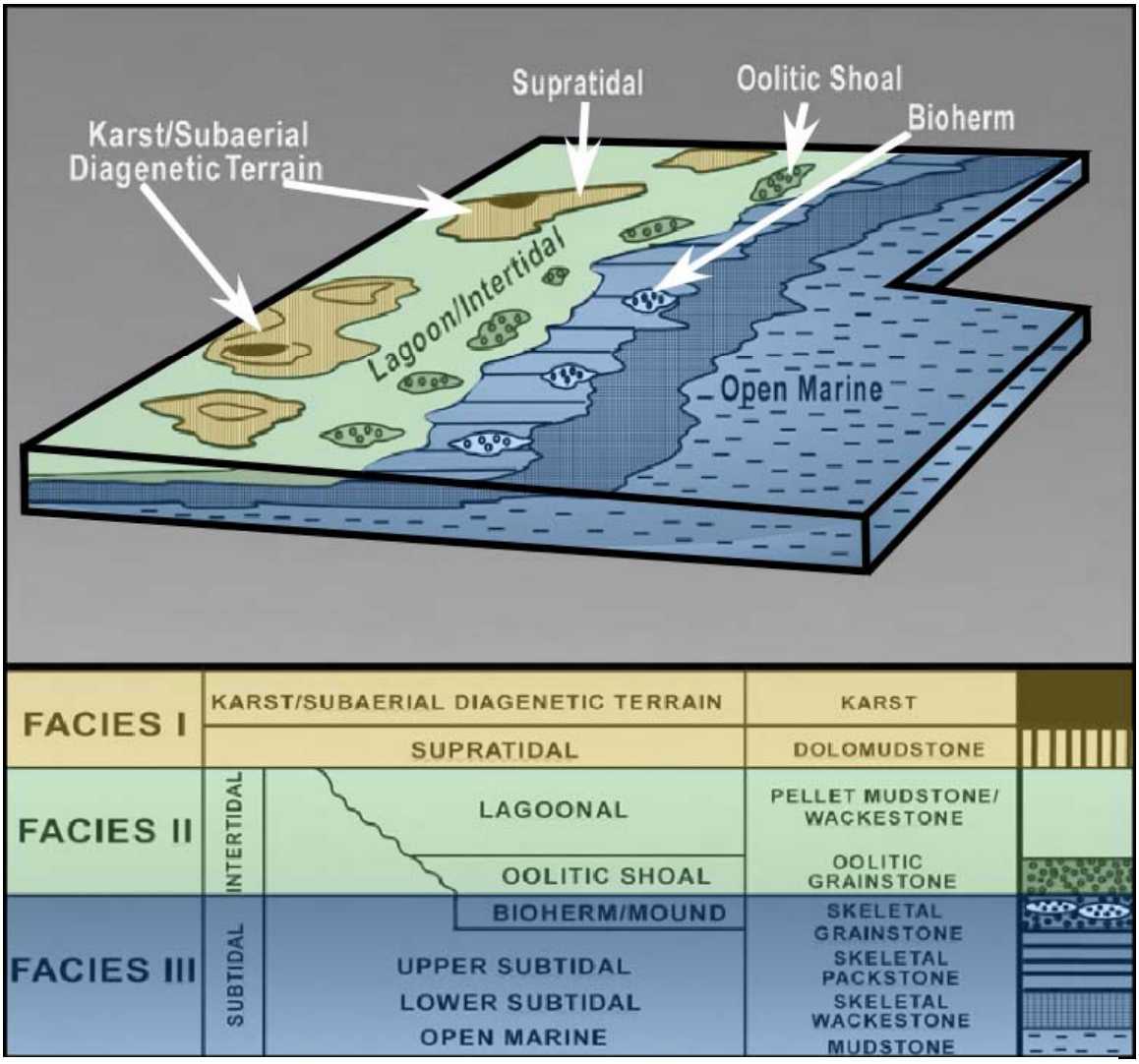

Figure 7. Hunton Group depositional facies model modified from Al-Shaieb (2000).

mudstone. The fauna within the open marine environment is primarily crinoid debris with minor amounts of mollusk and bryozoan debris. The unit experienced subsequent minor amounts of dolomitization (Al-Shaieb, 2000). Figure 8 illustrates the dolomitized matrix with abraded calcite bioclasts that are typical in an open marine environment.

The lower subtidal depositional environment falls in the middle of facies III. The lower subtidal unit is burrowed skeletal wackestone. Fossil abundance tends to decrease in the more argillaceous sediment (Mazzullo, 1978). The fauna in the lower subtidal environment is primarily crinoid debris with minor amounts of mollusk, bryozoan, brachiopod, ostracode, and trilobite fragments. The unit was burrowed and has been slightly dolomitized along the burrow traces. Figure 9 shows skeletal debris and burrows found in the lower subtidal environment.

The upper subtidal depositional environment is placed in the middle of facies III. The upper subtidal unit is a slightly dolomitized skeletal packstone. The fauna in the upper subtidal environment is primarily crinoid debris with minor amounts of bryozoan, trilobite, ostrocode, and brachiopod bioclasts. The unit is compacted, but contains enough matrix that skeletal fragments to have not generated sutured grain contacts. Figure 10 shows the fossil debris and dolomite found in the upper subtidal environment.

The bioherm/mound depositional environment is at the top of facies III. The bioherm/mound depositional environment has been studied in outcrop by Rechlin (2005), and has been described as a Waulsortian mud mound model (Wilson, 1975; Rechlin 2005). The mound depositional environment is restricted to the Frisco Formation (Fritz, 1994,Rechlin, 2005 part II). Growth was probably initiated on paleostructural highs

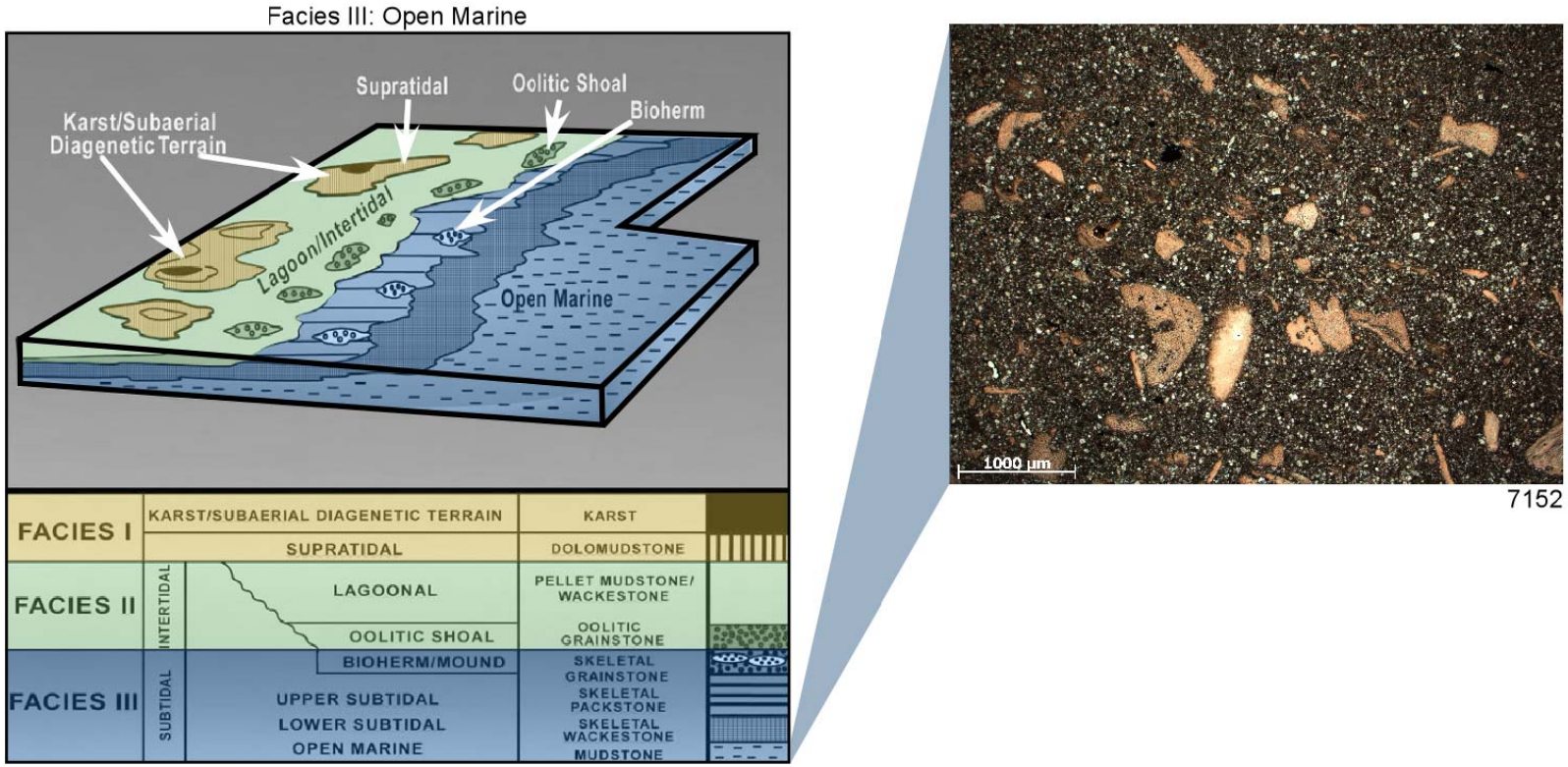

Figure 8. Thin section photomicrograph of open-marine carbonate with dolomitiezed matrix and abraded carbonate bioclasts (pelmatozoans). Plane-polarized light (PPL)

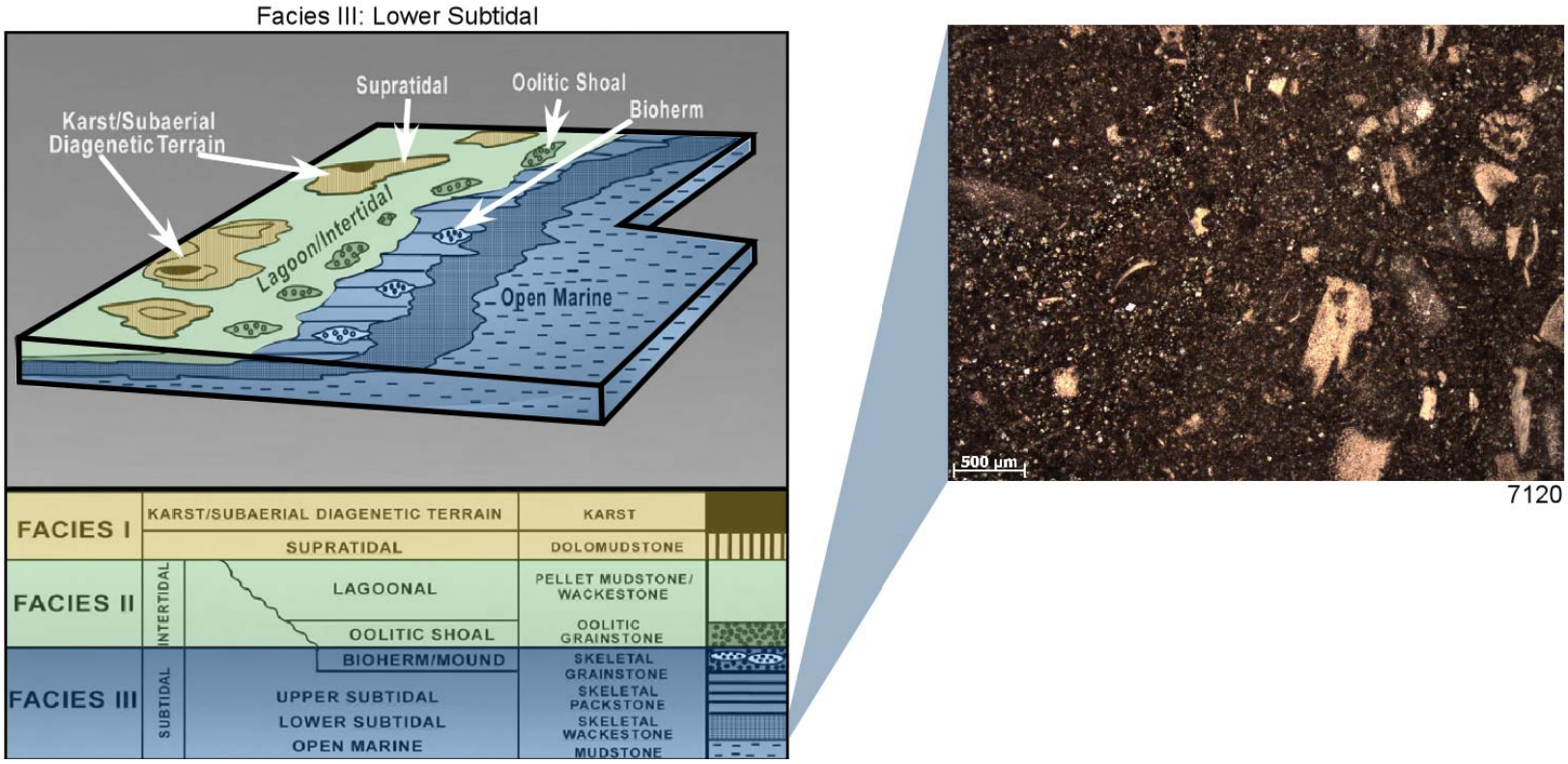

Figure 9. Thin section photomicrograph of lower subtidal carbonate with dolomitized burrows and abraded calcite bioclasts. (PPL)

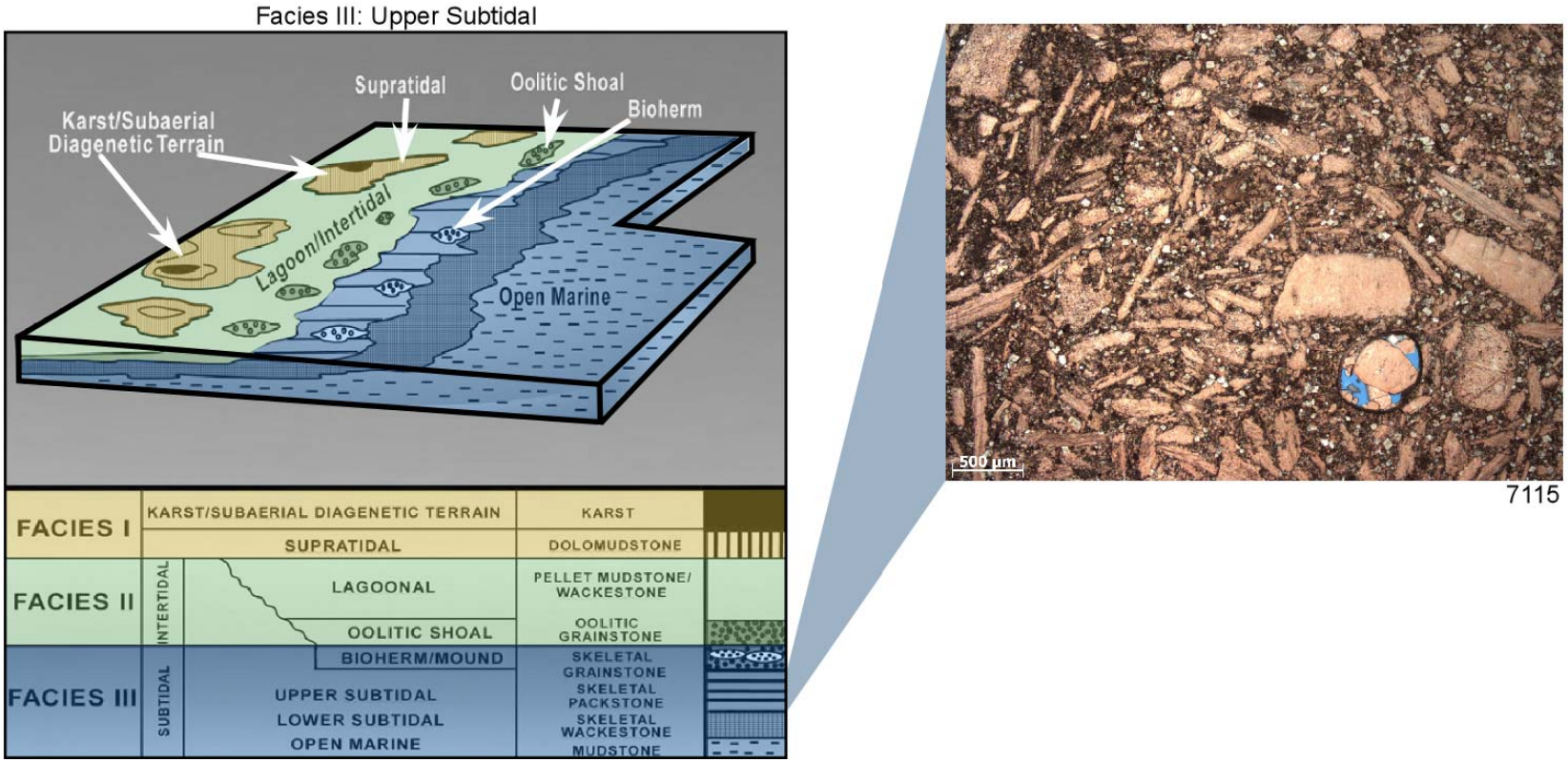

Figure 10. Thin section photomicrograph of upper subtidal carbonate with calcite bioclasts. (PPL)

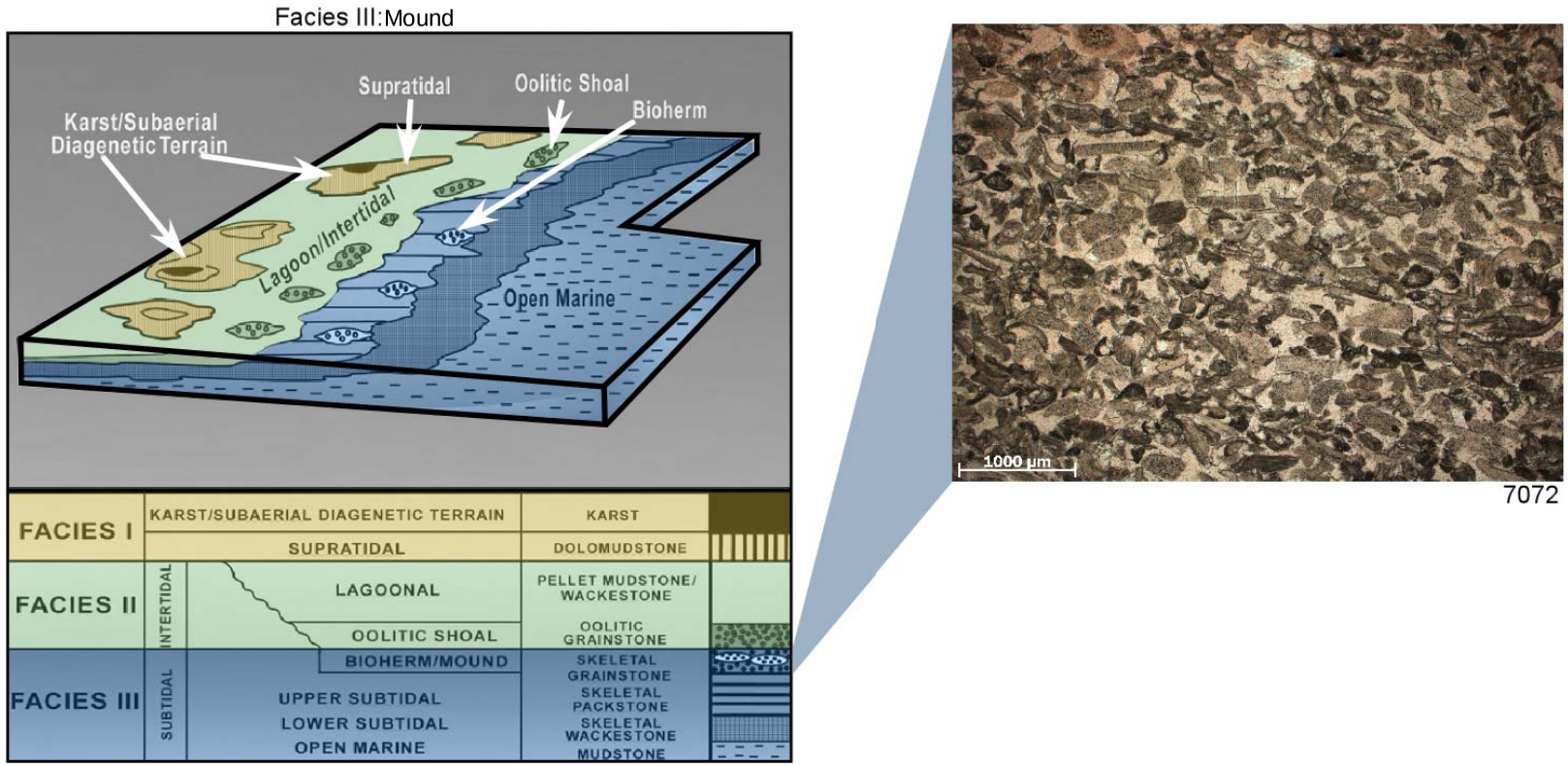

Figure 11. Thin section photomicrograph of mound carbonate with syntaxial calcite cement. (PPL)

(Medlock, 1987, Medlock, 1987, Rechlin, 2005 part I). The mound facies is a skeletal grainstone. The fauna in the mound environment is primarily crinoid and bryozoan debris with minor amounts of brachiopod, trilobite, and mollusk fragments. The crinoidal facies is commonly disseminated along the top and in front of bioherm buildups (Mazzullo, 1980). Early syntaxial calcite cement binds the fossil fragments. Figure 11 shows the skeletal debris and cement found in the mound environment as seen in thin section.

The oolitic shoal depositional environment is at the bottom a facies II. The oolitic shoal unit is a skeletal oolitic grainstone. The nuclei of the ooids are crinoid fragments and other indeterminate bioclastic debris. The development of ooids is connected to turbulence of a thin layer of hypersaline water oscillating over a shallow margin (Bathurst, 1975). Based on modern analogues, the optimum conditions for ooid growth are a water depth of 1.8 meters (Bathurst, 1975). Early syntaxial calcite cement occludes intergranular porosity. Figure 12 is a thin section photomicrograph showing the ooids and cement of the oolitic shoal environment.

The supratidal depositional environment is positioned at the bottom of facies I. The supratidal unit is a skeletal dolomitic mudstone to crystalline dolomite. The unit is partially to near completely dolomitized. The dolomite crystals are small rhombohedra with cloudy centers that are distinctive of hypersaline dolomite (Al-Shaieb, 2000). Hunton dolomite that formed in the near-surface environment underwent diagenesis associated with unconformity development (Sternbach, 1986, Kopaska-Merkel, 1989). The faunal debris in the supratidal environment is primarily abraded crinoid and mollusk fragments. Figure 13 shows the fossil debris and the crystalline dolomite.

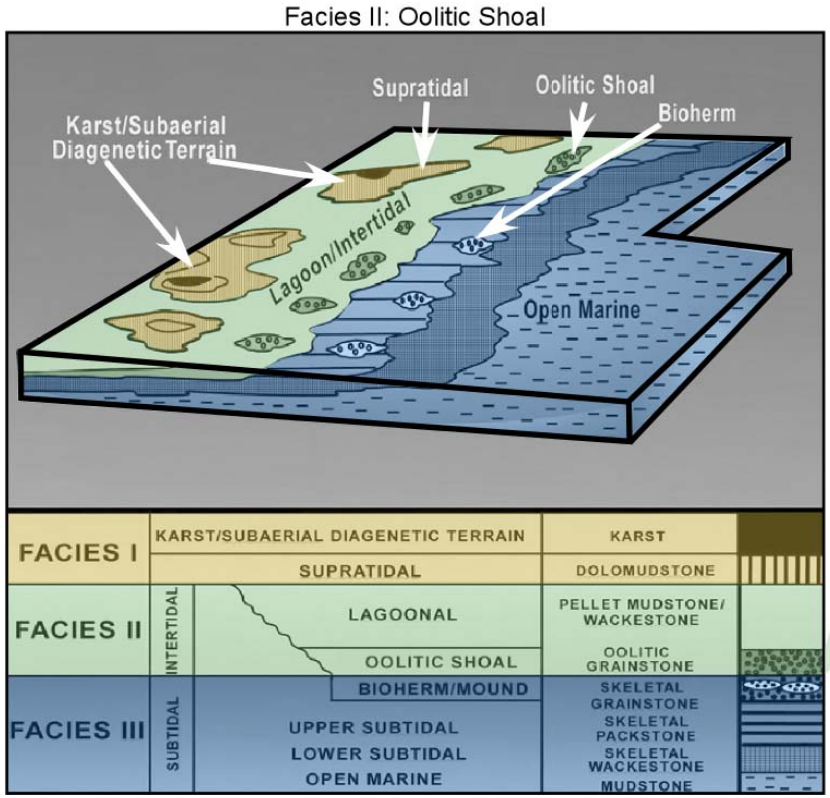

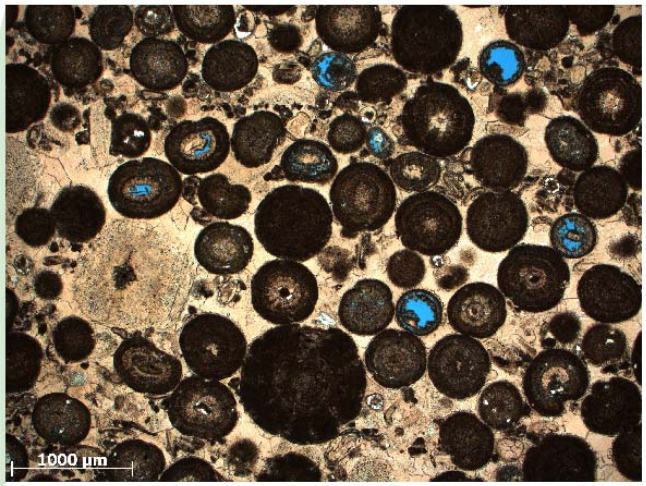

Figure 12. Thin section photomicrograph of oolitic shoal carbonate with syntaxial calcite cement. (PPL)

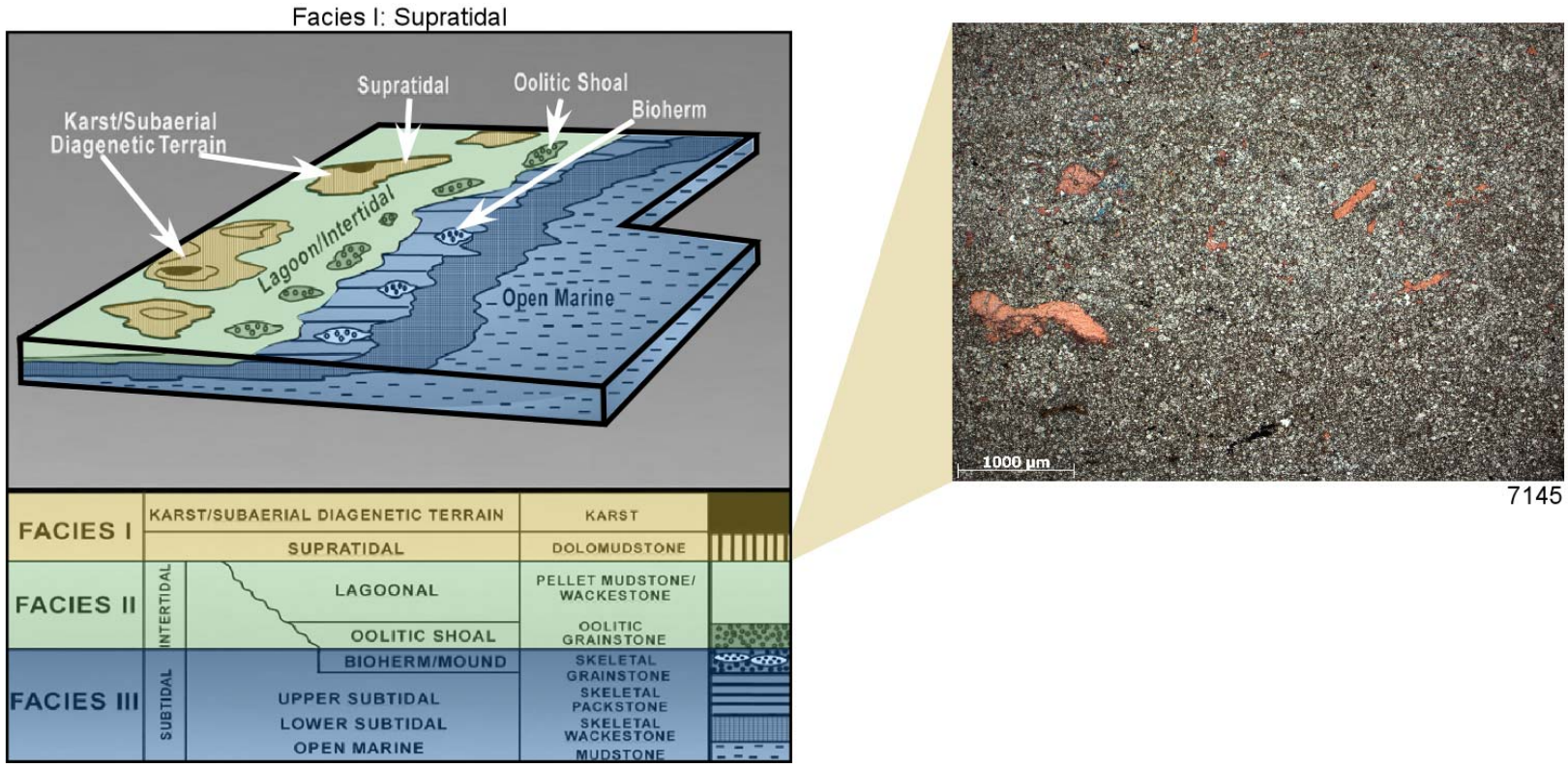

Figure 13. Thin secion photomicrograph of supratidal carbonate wi dolomitized matrix and abraded calcite bioclasts (pelmatazoan). (PPL)

Figure 14 is a diagram on which the stacking pattern of the three facies is superimposed on resistivity and porosity wire-line logs from the West Edmond SWD 1-24. The base of the core is interpreted to be in the subtidal depositional environment. It is postulated a subsequent regression exposed facies III to the hyper saline conditions of the supratidal environment of facies I. The skeletal oolitic grainstone marks a minor transgression and a shift from facies I to facies II. The ooid shoal was deposited within the high energy intertidal zone and above the normal wave base. The oolitic shoal is overlain by dolomudstone that marks a minor regression and juxtaposition of the supratidal depositional environment on facies II. The dolomudstone is overlain by a skeletal packstone that demarcates a transgression to facies III. Facies III is interrupted at 7,091 ft. by a break directly to facies I that represents a drop in sea level and slight regression to a supratidal environment. The dolomudstone of facies I is overlain by a skeletal packstone that marks a transgression to a subtidal depositional environment (facies III). The pre-Woodford unconformity truncates the facies succession. Depositional facies can be correlative to porosity and permeability, which is tied to textural variation (Houseknecht, 1992).

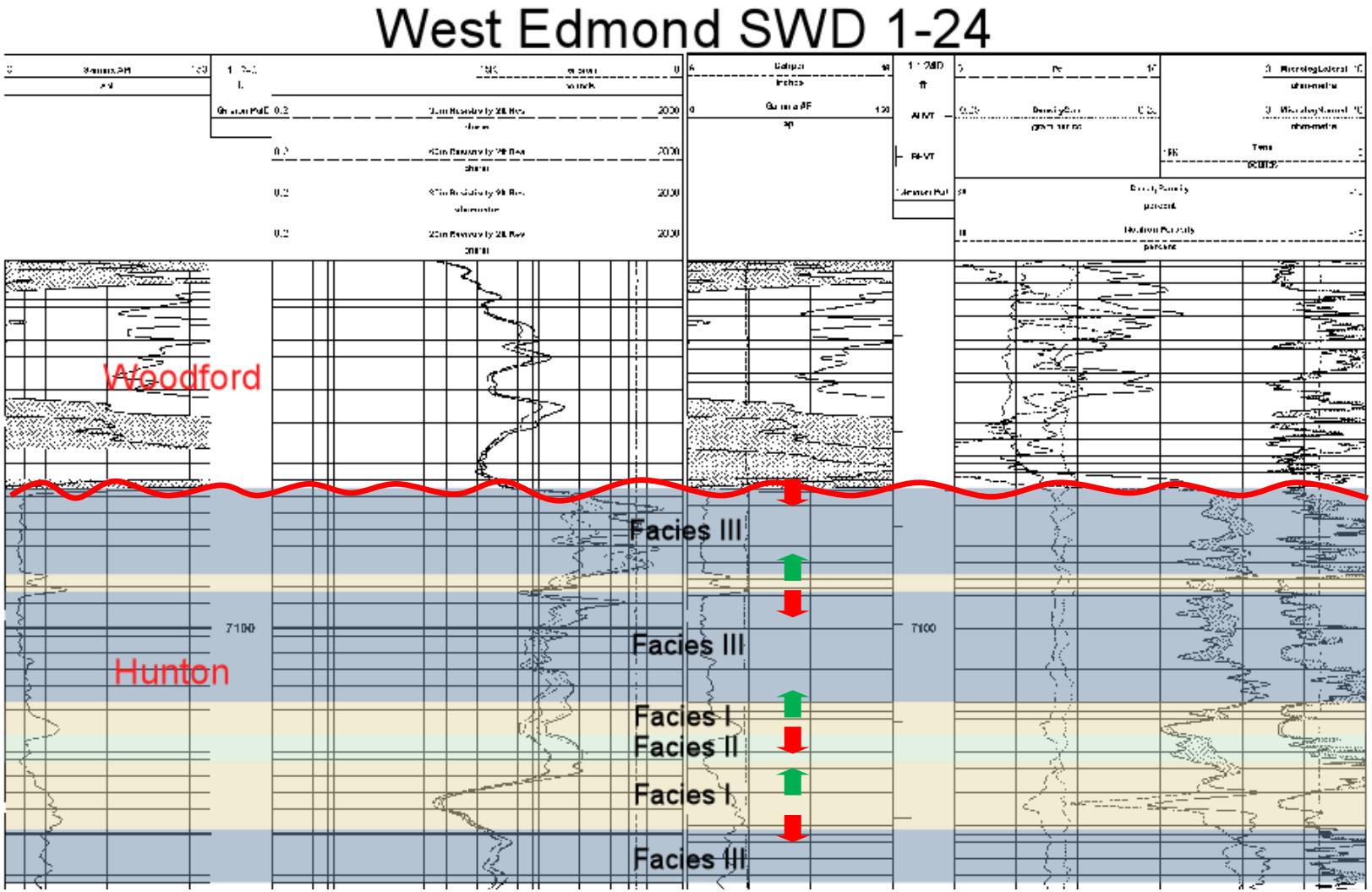

Figure 14. HuntonGroup depositional facies superimposed on West Edmond SWD 1-24 wire-wine logs. Red arrows represent interpreted fallingsea level and green arrows represent rising sea level.

CHAPTER IV

WEST EDMOND FIELD DEVELOPMENT AND UNITIZATION

Field Discovery

The West Edmond Field was discovered by Ace Gutowsky, who drilled the Wagner #1 in the NW ¼ , NW ¼, SW ¼ of Sec. 32, T.14N. R.4W., Oklahoma County, Oklahoma. The Wagner # 1 was a Wilcox test and reached a total depth of 7,690 ft. on March 25th, 1943 (McGee, 1946). An indication of oil and gas was reported in the Hunton at 6,866 ft. and casing was set (McGee, 1946). On April 28th, 1943, the Hunton was perforated from 6,951-6,956 ft. The Wagner No. 1 flowed 522 barrels of oil in 24 hours through a 9/32 inch choke, with a reported bottom hole pressure of 3,110 pounds per square inch (McGee, 1946). Ace Gutowsky is credited with the discovery of the West Edmond Field using the "doodle-bug" method (McGee, 1946).

Initial Development

The average initial production of wells completed in the Hunton Group until 1946 was approximately 1,200 barrels of oil a day. Initial production of individual wells ranged from 25 barrels of oil per day to 4,800 barrels per day (McGee, 1946). The West Edmond Field was developed before the advent of porosity wire-line logs (Mateu, 2002). Porosity measurements were limited to coring reservoir and non-reservoir faces and estimating pore volume. Initial production showed isolated areas of wells with anomalous gas-oil ratios that were not related to time of completion or their structural location.

The main producing reservoir of the West Edmond Field is the Frisco Formation and the upper part of the pre-Frisco carbonates. In early wells the reservoir was called the "Bois d'Arc." Oil and gas production for the Frisco Formation and the pre-Frisco carbonates is not restricted to any one part of the mentioned productive units. There are scattered areas where the Henryhouse Formation and or the Chimneyhill Formation are dolomitized and contribute to production (Swesnik, 1945).

Initially wells were completed without stimulation. The common practice was to acidize each well with 1,000 to 1,500 gallons of acid to alleviate skin damage (McGee, 1946). Natural flow was obtained in nearly all wells after acid wash (Littlefield, 1947). In one example a well treated with 10,000 gallons of acid failed to flow and required swabbing for several days before returning to normal production (McGee, 1946). Large acid washes were deemed a failure and small acid washes (1,000 to 1,500 gallons) were

the common completion practice during the initial development of the West Edmond Field.

Peak drilling activity occurred in February, 1945, when 62 wells were completed (Littlefield, 1945). Peak oil production rate was 87,500 barrels of oil per day in September, 1945 (Lincoln, 1969). Seven-hundred thirty one wells in the West Edmond Field produced in excess of 53 million barrels of oil as of September 15, 1946 (Littlefield, 1945). There were approximately 750 wells drilled in the field to June 1st, 1947 (Swesnik, 1945). On July 29th, 1947, the West Edmond Field, which was owned entirely by Phillips Petroleum, was unitized by order of the Corporation Commission of Oklahoma; thereby forming the West Edmond Hunton Lime Unit (Swesnik, 1945) (Northcutt, 2002).

The first water production was reported on January 31st, 1944 in the Schmitz-Specht No. 1-3, (Sec.36, T.14N., R.5W.), (Littlefield, 1947). Seven months later, ten wells were producing water. By March 1st, 1945, 42 wells were producing water. Water encroachment continued and by April 1st, 1946, 132 wells were producing water; by September 15th, 1946, 157 wells were producing water (Littlefield, 1947).

Production as of January, 1967 from 754 Hunton wells was 106,033,000 barrels of oil (Northcutt, 2002). Littlefield (1947) estimated that the original oil in place was 600 million barrels of stock tank oil. The fracture network was estimated to contain 60 million barrels or 10% of the original oil in place (Littlefield, 1947). The recovery of oil from the fracture network is estimated at 70%, whereas the recovery of oil from intergranular porosity is estimated at 32% (Littlefield, 1947). The total recoverable reserves were estimated at 165 million barrels of stock tank oil (Littlefield, 1947).

"Bois d'Arc" Waterflood

Re-injection of produced water into the "Bois d'Arc" was initiated on July, 1949, on the west side of the field with the Jones 2, (Sec.17, T.13N., R.4W.), and the Mariner (Sec. 28, T.13N., R.4W.) (Lincoln, 1969). Thirteen additional wells were utilized to spread injection along the entire south area (Figure 15). Injection of water increased from about 4,800 barrels per day initially to 8,500 barrels per day, and reached a total of 9.2 million bbl by April, 1953 (Lincoln, 1946). Injection was diverted progressively to other depleted areas of the "Bois d'Arc" for disposal. Injection extended the 5 BWPD/well water front up to one and one-half miles east through the reservoir without creating an oil bank (Lincoln, 1946). Several wells showed significant increases in oil production, but it is not clear if this response resulted from the waterflood, or the application of artificial lift to wells previously shut-in or dead (Lincoln, 1969). A far greater number of wells were flooded within a few months to a year with no increase in oil production. The operation was judged to be unsuccessful, and attempts to waterflood the "Bois d'Arc" were abandoned in mid-1953.

Net water injection and influx into the 4 mile long area totaled about 8 million barrels from January 1, 1949, to May 1, 1953 (Lincoln, 1969). During this period, the water front advanced through about 2,300 acres as defined by wells producing more than 80% water (Lincoln, 1969).

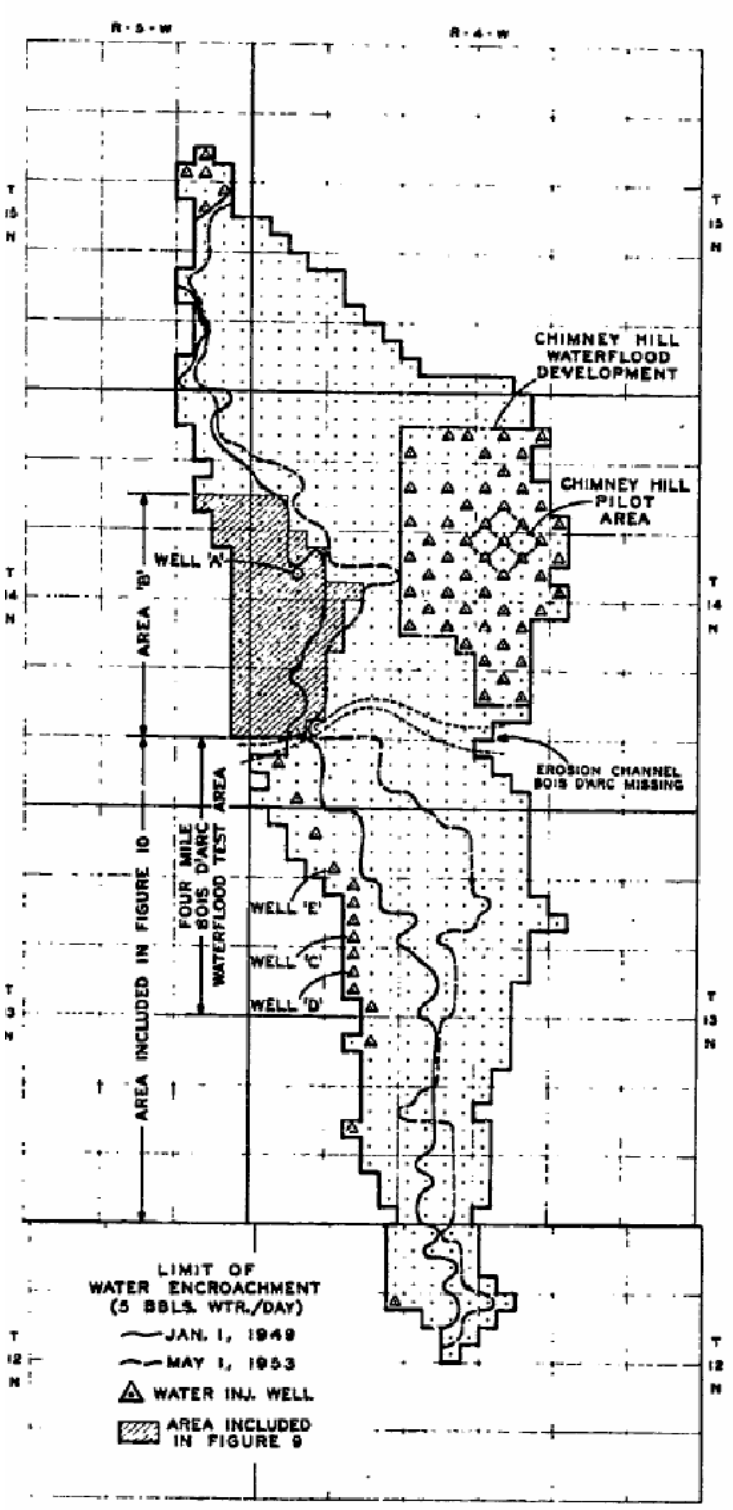

Figure 15. Map showing observations of the extent of water encroachment, the“Bois d’Arc” waterflood, “Bois d’ Arc” gas injection, and Chimney Hill gas injection pilot project. From Lincoln (1969).

When water injection into the "Bois d'Arc" was reduced starting August, 1953, and stopped altogether in February, 1954, oil production from the general area increased from 700 barrels per day to about 1,500 barrels per day in 15 months. Production leveled off at 900 to 1,000 barrels per day for 4 years—well above the decline trend during water injection (Lincoln, 1969).

The increase in oil production occurred primarily in wells at considerable distances behind the water front, wells that previously had produced large volumes of water at high water percentage. The wells gradually declined to about 50 % of the increase in production in 1964 (Lincoln, 1969). One former injector well, the Lynch #1 (Sec.5, T.13N., R.4W.), was returned to production in September, 1956 (Lincoln, 1969). During 1958, the Lynch #1 averaged 96 barrels of oil per day (Lincoln, 1969). By January, 1968, the Lynch #1 had recovered 131,500 barrels of oil after receiving more than 1 million barrels of water during injection (Lincoln, 1969).

Lincoln (1969) proposed that the large volume of oil produced behind the water bank could be the result of water being forced into the rock matrix where reservoir pressure increased. Rearrangement of fluids there permitted expulsion of additional oil when reservoir pressure was subsequently reduced. Such performance has been demonstrated in pressure pulsing of oil-wet cores in the laboratory (Lincoln, 1969).

"Bois d'Arc" Gas Injection

Between May and August 1948, 250 MMcf of gas was injected into the "Bois d'Arc" in the Stinchcomb A-1 (Sec. 28, T.13N., R.4W.). Two weeks after gas injection stopped, the gas-oil-ratio of the northeast offset declined from about 21,000 to 11,500 cu ft/bbl., and within a month the gas-oil-ratio of the east offset declined from 12,000 to 6,700 cu ft/bbl. (Lincoln, 1969). It is estimated that 43% of the gas was channeled to these wells (Lincoln, 1969). Most of the gas migrated away from the vicinity of the injection well without effectively displacing oil.

A second test was conducted in an area producing from only the "Bois d'Arc" near its up structure truncation. During 4 months, 383 Mcf/D of gas per day were injected into the West #4 (Sec. 15, T.13N., R.4W.), and the McClure #3 (Sec. 15, T.13N., R.4W.). The injection gas volume was increased throughout the duration of injection and a total of 476 MMcf was injected into the two wells (Lincoln, 1969). In March, 1948, these wells were shut in to conserve gas, and produced 10-60 barrels of oil per day per well with gas-oil-ratios of 10,000 to 80,000 cu ft/bbl, and averaged 30,000 cu ft/bbl (Lincoln, 1969). During 4 months of approximately balanced injection and production, these 5 wells averaged about 15 barrels of oil per day total at gas-oil-ratios of 125,000 to 275,000 cu ft/bbl. (Lincoln, 1969). Gas injection was stopped in July and the wells produced the same total gas production. Over a 10 week period oil production of the 5 wells increased gradually from 15 to 70 barrel of oil per day total, and the composite gas-oil ratio

declined from 250,000 to 50,000 cu ft/bbl. (Lincoln, 1969). Analysis of the changing gas-oil ratios resulted in the interpretation that the main flow channels constitute about 8% of the reservoir space (Lincoln, 1969).

Helium was added to injection gas as a tracer at 1% concentration for a week starting April 27, 1948 (Lincoln, 1969). Helium was detected in 12 days, and in seven of the nine test wells during the 5 month test (Lincoln, 1969). About 44% of the injected helium was produced (Lincoln, 1969). If peak helium content corresponds to average travel times of injected gas to the various wells, and if all gas flow was confined to the 160-acre area enclosed by the affected wells, then minimum reservoir volume swept by injected gas was about 6% of the reservoir pore space (Lincoln, 1969).

In a third test, gas was injected into the "Bois d'Arc" in the Lenhart B-4 (Sec 30, T.15N., R.4W.), and Messenbaugh #4 (Sec. 30,T.15N.,R.4W) (Lincoln, 1969). These wells and their offsets were shut-in on December, 1947, and essentially all of T.15N. was shut in through early 1950 (Lincoln, 1969). Injection into the Messenbaugh #4 started March 23, 1948, at 580 Mcf/D and ranged up to 2,900 Mcf/D (Lincoln, 1969). A total of 128 MMcf was injected through June 4, 1948 (Lincoln, 1969). Injection into the Lenhart B-4 started on April 1, 1948 at 780 Mcf/D and increased successively to 6,500 Mcf/D by June 23, 1948. The test was stopped after cumulative injection of 267 MMcf (Lincoln, 1969). Within 6 weeks the pressures stabilized between the injection wells and shut-in wells.

Reasonable agreement between calculated and measured effective permeabilities to gas in the range of 4.5 to 6 millidarcies and associated effective porosities to gas range from 3% to 2% (Lincoln, 1969). Porosity measured by pressure interference in the 3

month test is one-third to one-half the total porosity. This is a further indication of limited flow channels in a low permeability matrix (Lincoln, 1969).

Chimney Hill Gas Injection

A fourth pilot test involved injection of 571 MMcf of gas into only the Chimney Hill section in the Shinn 1 (Sec. 22, T.14N., R.4W.) and measuring gas and oil production from the 8 offset wells. Nearly all of the latter wells were perforated in both the "Bois d'Arc" section and Chimney Hill section. Two weeks after gas injection was stopped, the gas-oil-ratio of the northeast offset declined from about 8,500 to 7,500 cu ft/bbl (Lincoln, 1969). Less than 5% of the daily gas injection was recovered (Lincoln, 1969). The injected gas produced an effective oil bank. No other tests in the West Edmond Field showed such a reduction in the gas-oil-ratio. The degree of fracturing in the Chimney Hill is inferred to be considerably less than that indicated for the "Bois d'Arc" section by the results of pilot gas injection tests (Lincoln, 1969).

A bulk of the initial oil and gas production is believed to come from an interconnected network of solution-enlarged fractures that are present throughout the "Bois d'Arc" (Swesnik, 1945). Porosity and permeability measured in Hunton wells in the West Edmond Field on average are low for oil-producing zones (Swesnik, 1945). Observations made on the rig floor while the pay zone was being drilled and

conversations with drillers about other wells in the field led to the inference that soft spots or solution channels are present. Soft spots are shown by a sudden increase in the number of points on the weight indicator. When they are encountered, drillers decrease pressure on the brake, thus lowering the drill string several inches in order to return to the normal reading on the weight indicator. Soft spots of a few inches up to more than a foot were observed. Rate of penetration of the drill bit is erratic through the pay zones (Swesnik, 1945). It is thought that solution channeling, although not in an advanced stage to initiate karst topography was the most important factor in the formation of the porosity in the "Bois d'Arc" of the West Edmond Field (Swesnik, 1945). The contrast between severe water channeling in the "Bois d'Arc" and profitable water-flooding in the Chimney Hill Formation demonstrates the need for detailed geologic description of reservoir rocks and developing an understanding of the distribution and movement of fluids within the reservoir.

CHAPTER V

PETROPHYSICAL ANALYSIS OF RESERVOIR AND NON RESERVOIR

Thin Section Pore Analysis

A petrophysical classification of the reservoir and non-reservoir rocks in Hunton carbonates is based upon thin section analysis of the core from the West Edmond SWD 1-24, (Sec. 24, T.14N., R.4W.). Examination of lithofacies leads to definitions of petrophysical facies. An important component of reservoir characterization is the description of the pore system (Kopaska-Merkel, 1989). Sixty-six thin sections and 25 enlarged thin sections were made by Wagner Petrographic from selected samples. Both types of thin sections were prepared with one half of the thin section stained with alizarin red and one half of the thin section unstained. The 66 thin sections were taken from the 66 core plugs used for permeability calculations. Each thin section was analyzed and classified using the Dunham carbonate classification (Dunham, 1962) shown in Figure 16. Porosity types were classified using the Lonoy carbonate porosity classification shown in Figure 17 (Lonoy, 2006).

The most widely used pore-type classification systems for carbonate reservoirs are limited by the fact that the relationship between porosity and permeability is poorly defined (Lonoy, 2006). The porosity classification system most widely used by carbonate

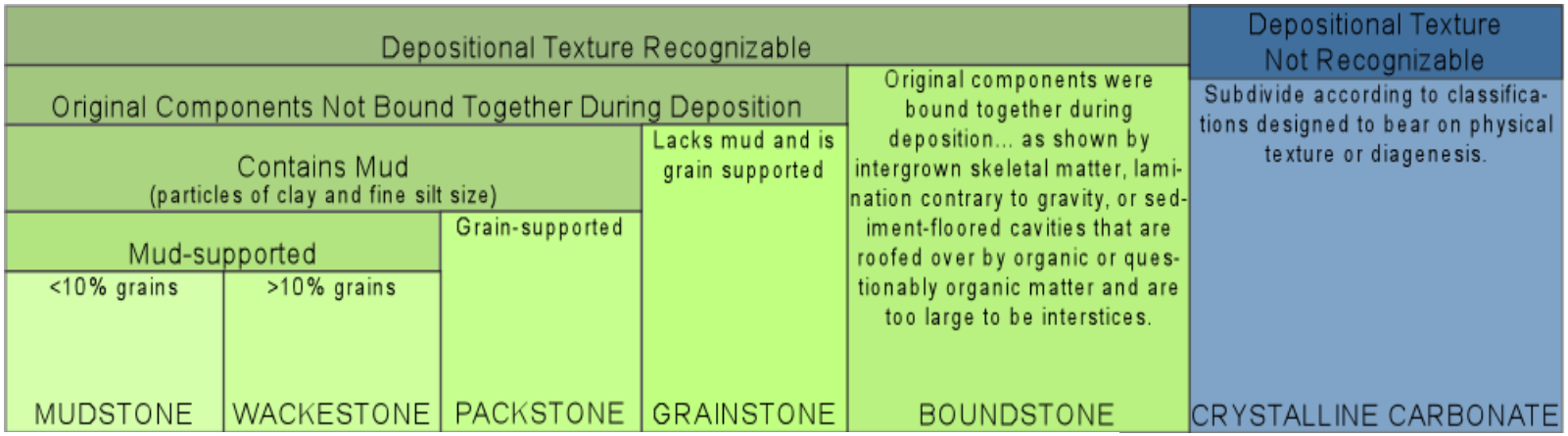

Figure 16. Dunham carbonate classification (1962).

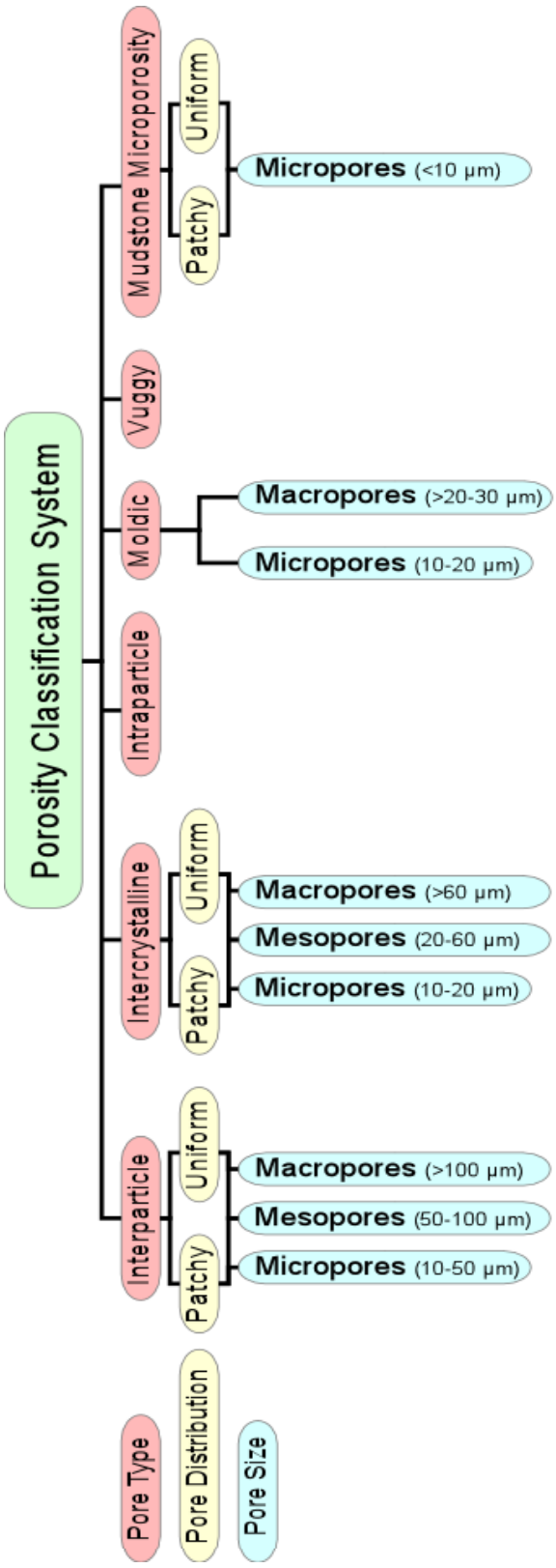

Figure 17. Lonoy carbonate porosity classification (2006).

petrographers and petroleum geologists is the one developed by Choquette and Pray (1970). The Choquette and Pray porosity classification system links sedimentological fabric and pore types, thus pore types can be predicted based upon depositional setting and/or diagenetic evolution (Choquette, 1970). The Archie (1952) and Lucia (1983, 1995, 1999, 2003) porosity classification systems are directly linked to pore geometries and flow properties (Lonoy, 2006). The pore-type classification used for this study incorporates elements of both rock texture and pore size, reflecting depositional and diagenetic fabrics (Lonoy, 2006). As such, it builds from the important work of Choquette and Pray (1970), Lucia (1983, 1995, 1999), and Lonoy (2006).
The Lonoy carbonate porosity classification system combines sedimentological and diagenetic features with flow-related properties that allow porosity to be predicted using sedimentologic and diagenetic models (Lonoy, 2006).

Three pore types dominate the rocks in thin sections in discrete parts of the core and are thus separated into three units. Intraparticle porosity, intercrystalline porosity, and moldic porosity are the three dominant pore types observed in thin sections. Each porosity type is distinctive to a given unit in the Frisco Formation and the pre-Frisco carbonates of the West Edmond Field.

Skeletal grainstones and packstones have predominately intraparticle porosity Intraparticle pores are pore spaces occurring within grains that are primary in origin or from the decay of organic material. Interparticle pores are associated with medium to high energy depositional settings (Lonoy, 2006). Intraparticle pores are abundant in the zooecia of bryozoa and occasionally within the central canal of crinoid fragments (Moore, 2001). The crinoid fragments tend to be replaced pseudomorphically on a

volume-for-volume basis, and probably undergo little compaction. The effect of the crinoid fragments on the original porosity of the rock will be to reduce the porosity because solid crinoid fragments and their syntaxial calcite overgrowth take up space which would otherwise be occupied by bryozoan fragments with intraparticle porosity (Lucia, 1962). Reducing porosity causes escalating constrictions of pore throats and increasing tortuosity of flow paths resulting in a decline in permeability (Budd, 2002).

The intraparticle porosity is assumed to be primary porosity and many times is patchy and dissolution enlarged. Dissolution progressed through complete removal of some interstitial material and partial removal of component particles. Selective dissolution of cements and matrix is strongly controlled by fluid migration pathways (fractures, permeable zones), which yield a patchy pore distribution. Patchy cement distribution is commonly controlled by selective precipitation of syntaxial calcite cement overgrowths on a single crystal grain. Syntaxial calcite cement typically nucleates on an echinoderm fragment. Patchy intercrystalline pore distribution related to texture is associated with early diagenesis.

Diagenesis is a function of pressure, temperature, the nature of the fluid moving through the sediment, and the physical and chemical nature of the original sediment. Pressure and temperature are fairly constant over a broad area. Diagenetic changes on a smaller order are a variation in the nature of the formation fluid and or variations in the physical or chemical nature of the original sediment. The permeability of intraparticle porosity is low do to the relative isolation of pore spaces unless dissolution processes enlarged pore spaces and etched pore throats. Figure 18 shows intraparticle porosity as seen in thin section from the West Edmond SWD 1-24.

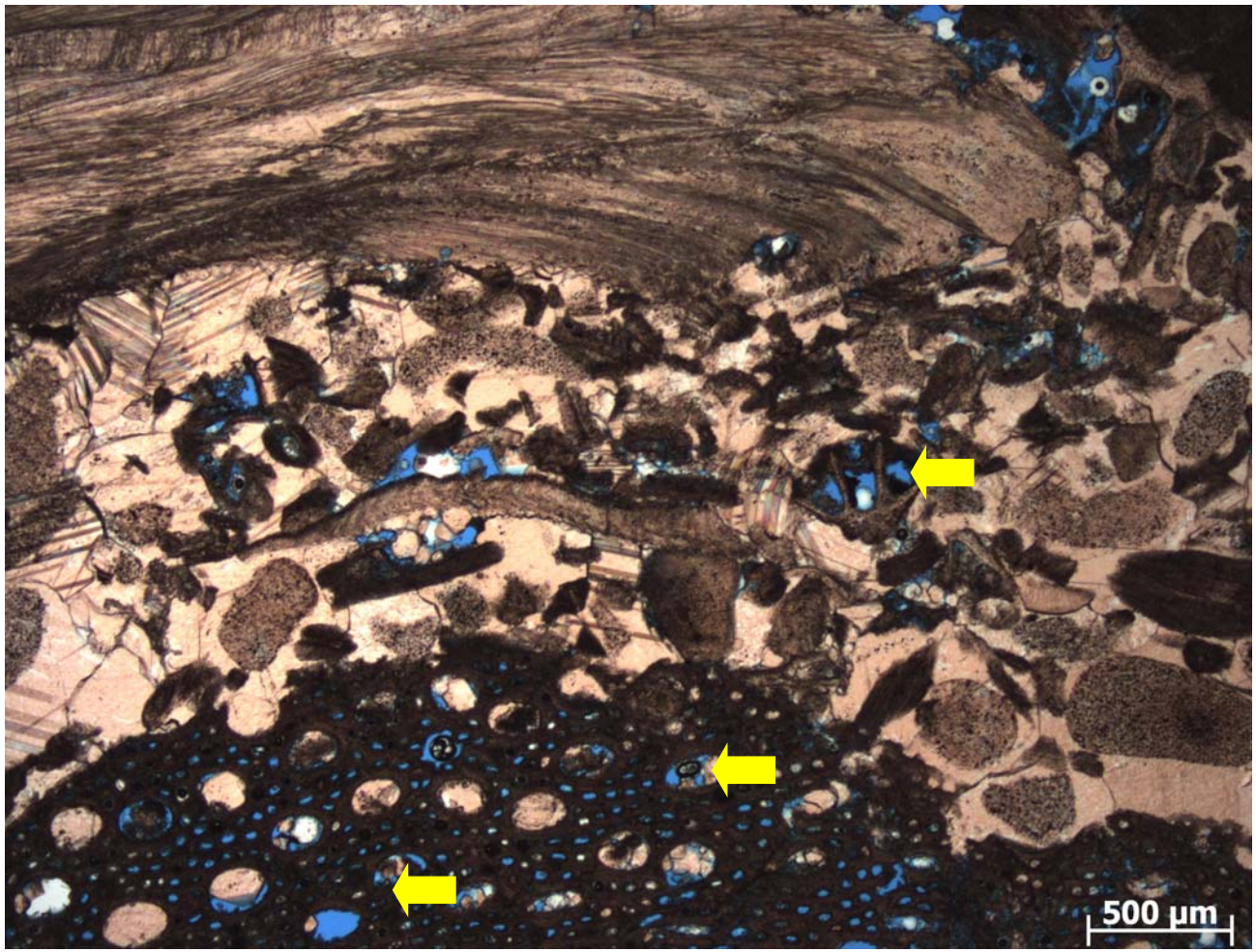

Figure 18. Intraparticle porosity in bryozoans fragment (arrows) at 7,100 ft. from West Edmond SWD 1-24 (5% porosity and 2.2md permeability). Pore space is filled with blue epoxy. (PPL)

Dolomitized skeletal wackestones have predominately intercrystalline porosity. Intercrystalline porosity is pore structure that is controlled by dolomite crystals. Dolomitization frequently increases the petrophysical maturity of porosity in fine-grained carbonates (Roehl, 1967). Finely crystalline rocks develop permeability as the dolomite content increases. The amount of carbonate in natural waters is small in comparison with the amount of magnesium and calcium. The carbonate used to form secondary dolomite must come from the calcite or aragonite in the sediment (Weyl, 1960, Lucia, 1962). In order that a porous dolomite is produced through dolomitization, the volume of carbonate used must be limited to an amount essentially equal to the volume that present in the original calcite and aragonite (Murray, 1960, Lucia, 1962). If additional carbonate is added from outside the rock being dolomitized, the volume of the dolomite formed could be greater than the volume of calcite and aragonite replaced, and porosity would thus decrease in proportion to the amount of additional carbonate added to the system. (Murray, 1960, Lucia, 1962). The difference in volume between calcite and dolomite will be compensated by compaction until the dolomite crystals form a supporting framework (Weyl, 1960). Dolomite crystals, crinoid fragments, or other skeletal material form the supporting framework, thus, the amount of supporting framework material in the original sediment will affect the time at which the compaction related dolomitization stops and the porosity of the original sediment is preserved (Lucia, 1962).

Intercrystalline micropores are 10-20 μm in diameter. Intercrystalline mesopores are 20-60 μm in diameter. Intercrystalline macropores have diameters greater than 60 μm. It is difficult to estimate the intercrystalline pore size through a petrographic microscope. The visible pores in thin section are believed to be either mesopore to macropore size.

The permeability of intercrystalline porosity is dependent upon the pore size. The larger the average pore size the better the permeability. Figure 19 shows intercrystalline porosity as it appears in thin section from the West Edmond SWD 1-24.

Moldic micropores are less than 10-20 μm. Oolitic grainstones have predominately moldic porosity. The oolitic grainstone is a fragmental limestone with a complete or partial matrix of crystalline early syntaxial calcite cement. Solution has affected both the matrix and the ooids. The ooids that form the moldic porosity have undergone dissolution; ergo, creating an ooimold. Moldic porosity can be divided into moldic micropores or moldic macropores. Moldic micropores are less than 10-20 μm. Moldic macropores are larger than 20-30 μm. The permeability of moldic porosity is poor do to the large isolated pore spaces. Figure 20 shows moldic porosity as seen in thin section from the West Edmond SWD 1-24.

Other porosity types are present in the Frisco Formation and pre-Frisco carbonates, but the volume of the porosity that they represent is small compared to the volume of intraparticle porosity, intercrystalline porosity, and moldic porosity found within their respective lithologies. Fracture porosity and solution-enlarged porosity is visible at the thin section scale. The importance fracturing and solution-enlarged porosity cannot be understated. Intraparticle porosity, intercrystalline porosity, and moldic porosity have relatively low permeabilities compared to fracture permeability. Fracture porosity networks are believed to connect low permeability intraparticle porosity, intercrystalline porosity, and moldic porosity.

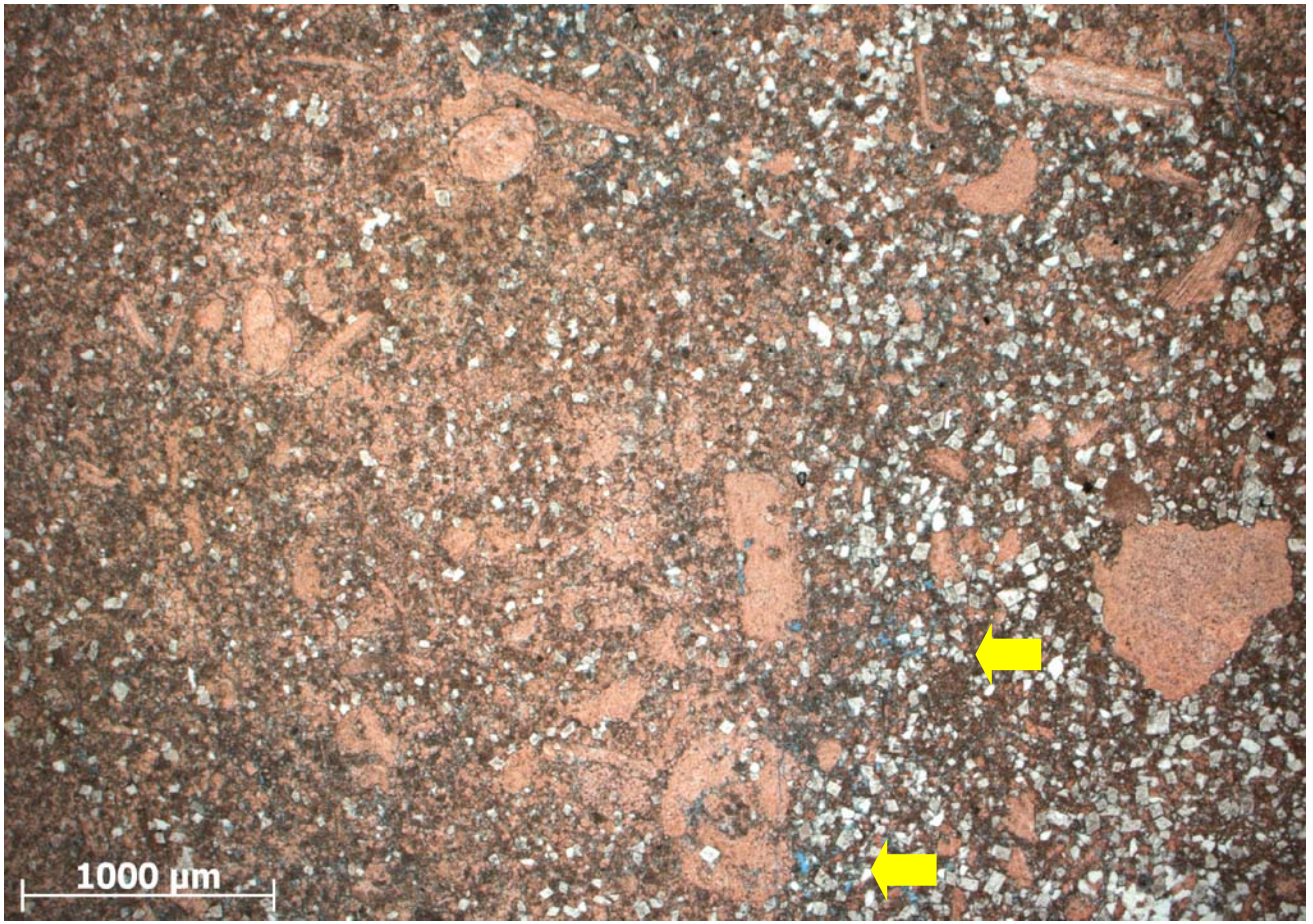

Figure 19. Intercrystalline porosity between dolomite crystals (arrows) at 7,122 ft. from West Edmond SWD 1-24 (9% porosity and 1.5 md permeability). Pore space is filled with blue epoxy. (PPL)

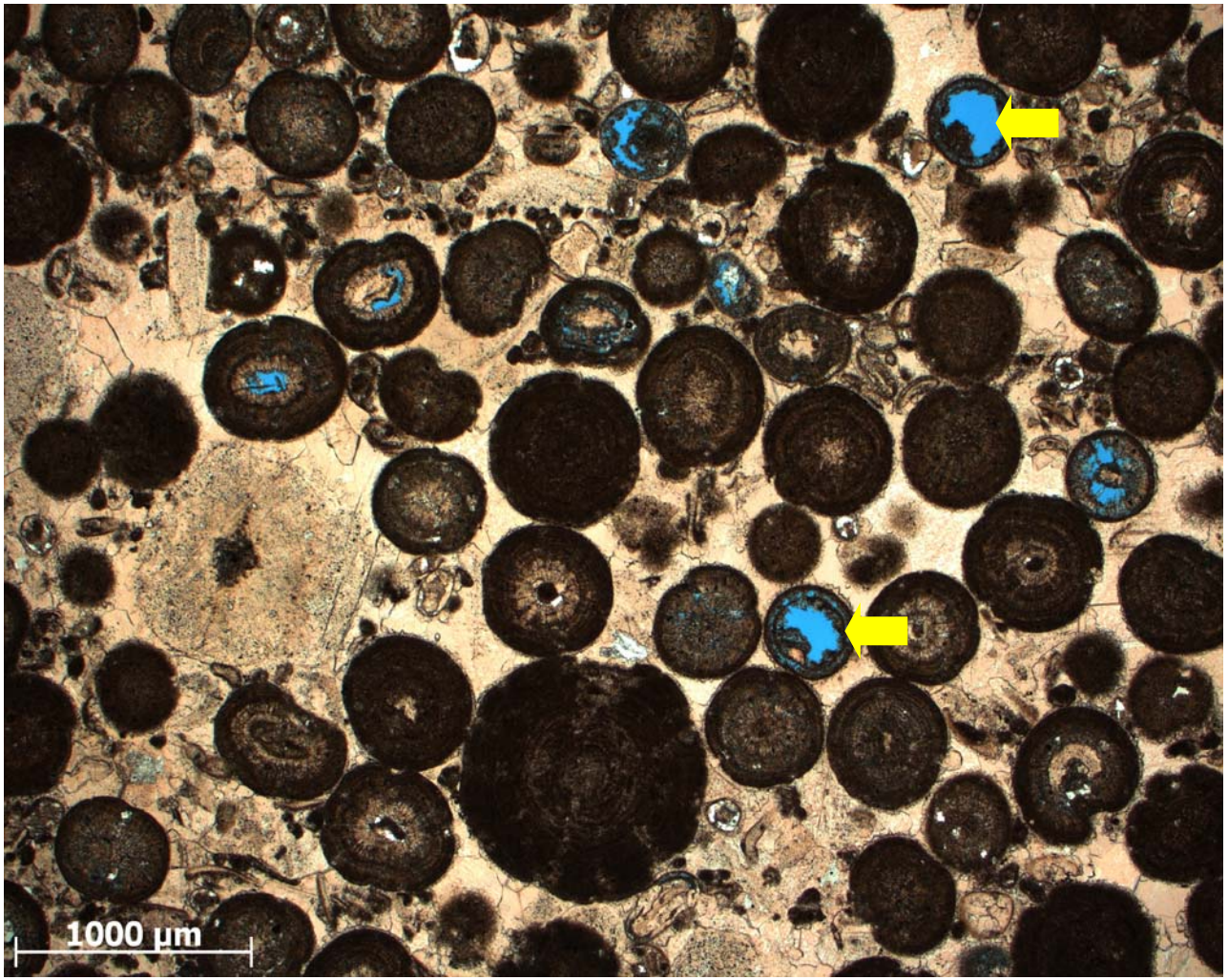

Figure 20. Oomoldic porosity forming within ooids at 7,133 ft. from West Edmond 1-24 (2% porosity and 0.6 md permeability). Pore space is filled with blue epoxy. (PPL)

Scanning Electron Microscopy

Six samples were selected and analyzed with the scanning electron microscope (SEM) in the Chesapeake Reservoir Technology Center. The SEM images were taken by Rick Urash at the Chesapeake Reservoir Technology Center. The SEM images were of samples that were located in skeletal packstones and dolomitized skeletal wackestones. The SEM photographs were analyzed for porosity that is not visible at the core or thin section scale.

Sample 1 from 7073.9 ft. is a skeletal packstone. Figure 21 shows a relatively coarse calcite spar and minor dolomite. Intercrystalline porosity (blue arrows) occurs primarily in dolomitic zones. Intercrystalline porosity (green arrows) is a patchy minor component of the pore system. Figure 22 and Figure 23 illustrate intercrystalline pores are partially filled with authigenic illite (IL) and lined with a carbonate cement (orange arrows). The intercrystalline pores are 10 μm-20 μm in width. The intercrystalline porosity system in sample 7073.9 ft. is patchy. Patchy porosity yields a significantly higher permeability (Lonoy, 2006). The patchy porosity is concentrated over a smaller volume, thus and the pore system is better connected than a uniformly distributed pore volume (Lonoy, 2006). Patchy porosity distribution is often related to secondary dissolution and the slight corrosion of pore throats, which favors connected pore throats (Lonoy, 2006).

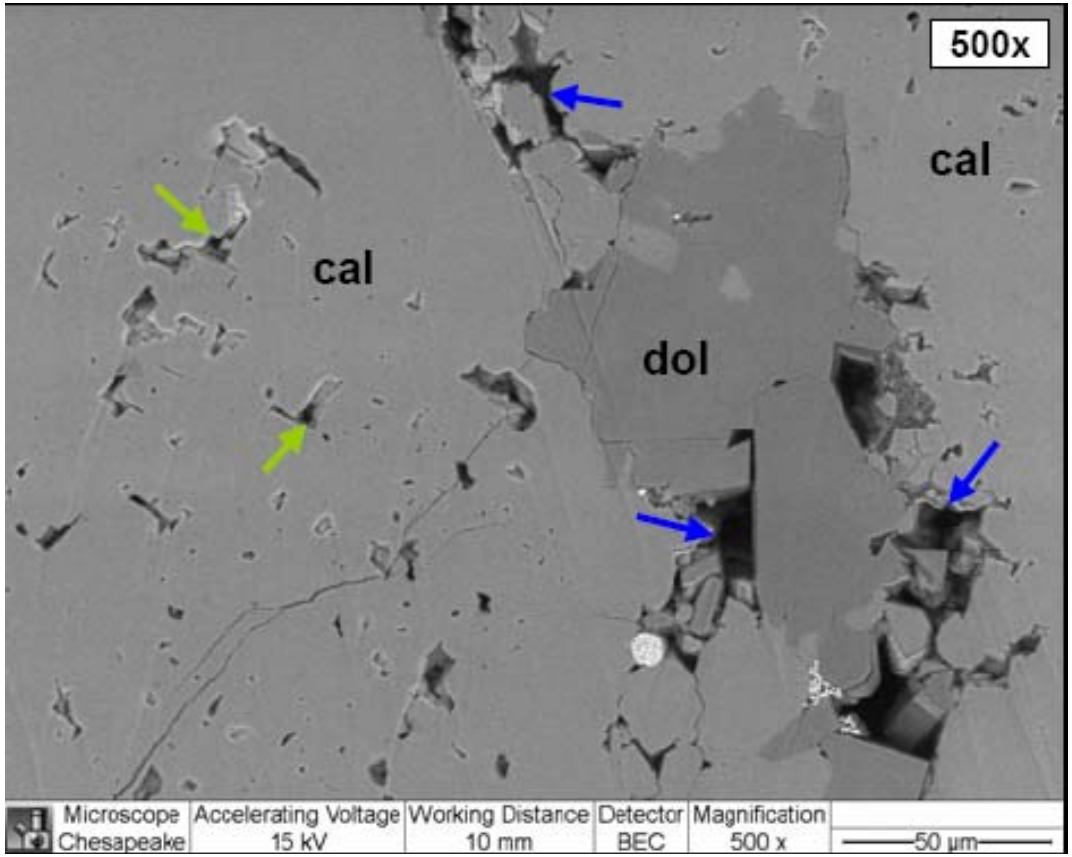

Figure 21. Scanning electron microscope image at 7073.9 ft. at 500x. Dolomite (dol) and calcite (cal) make up the skeletal wackestone. Dolomitic intercrystalline porosity indicated by the blue arrows and patchy intercrystalline pores found in calcite are shown by the green arrows. Image taken by Rick Urash at Chesapeake Energy Reservoir Technology Center.

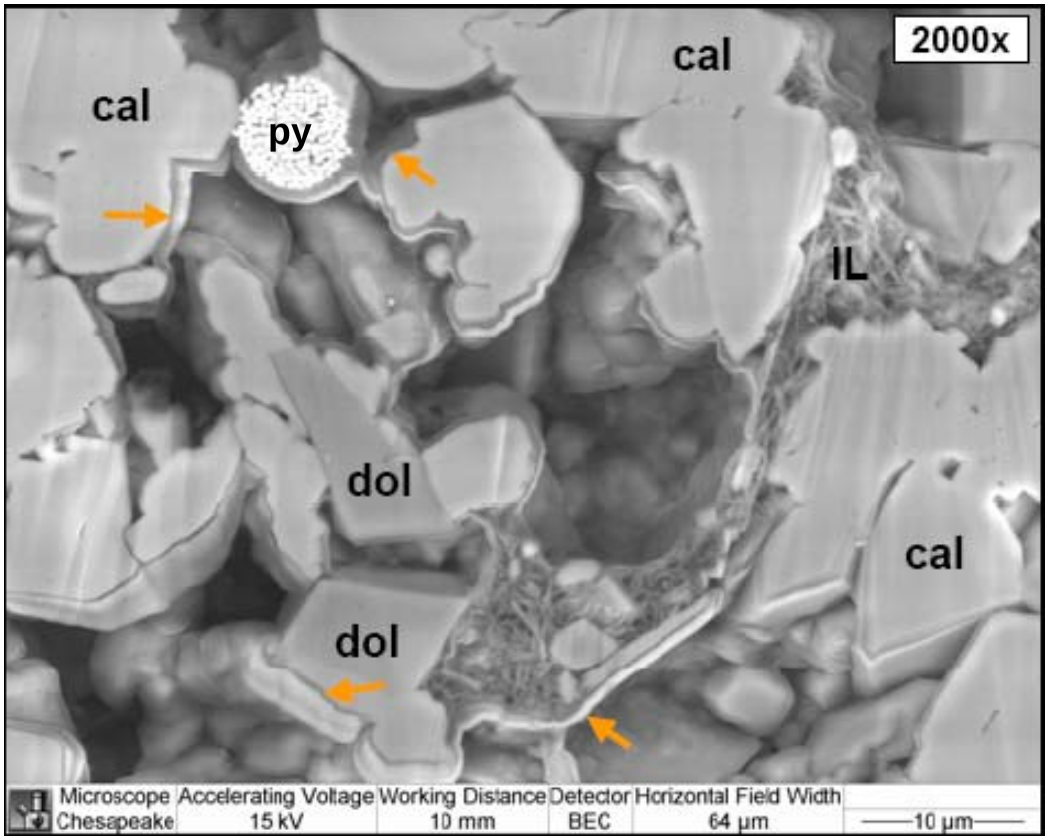

Figure 22. Scanning electron microscope image at 7073.9 ft. at 2,000x. Dolomite (dol) and calcite (cal) make up the skeletal wackestone. Authigenic illite (IL) flkes partially fill pores and are lined with a carbonate cement (orange arrows) Framboidal pyrite (py) "golf balls" are a minor constituent of the sample. Image taken by Rick Urash at Chesapeake Energy Reservoir Technology Center.

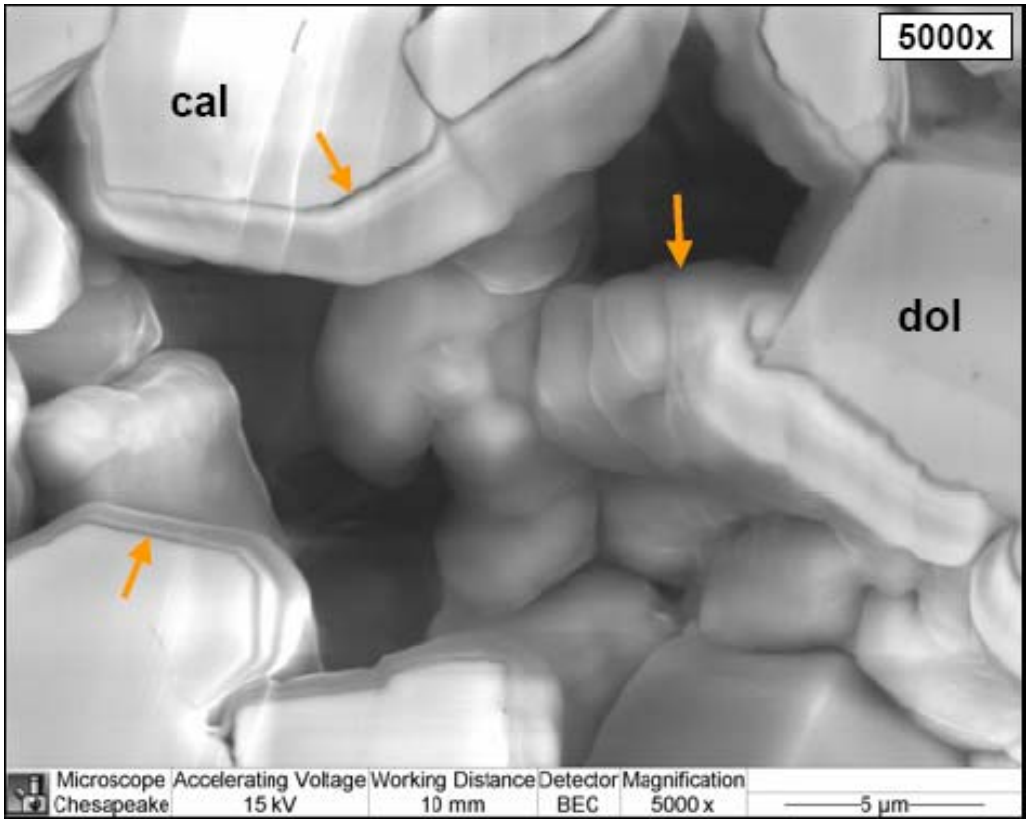

Figure 23. Scanning electron microscope image at 7073.9 ft. Image at 5,000x. Dolomite (dol) and calcite (cal) make up the skeletal wackestone. Pores are lined with calcite cement (orange arrows). Image taken by Rick Urash at Chesapeake Energy Reservoir Technology Center.

Sample two from 7128.6 ft. is a dolomitized skeletal wackestone. The area shown in Figure 24 has significantly more dolomite (dol) and intercrystalline porosity (green arrows) than the previous sample shown in Figure 21. Unique to this sample are vuggy pores (white arrows) up to 100 μm in diameter. The carbonate cement (orange arrows) shown in Figure 25 commonly lines large intercrystalline pores. This carbonate cement could be an indication of fluid flow through the pore network and effective porosity. Authigenic illite shown in Figure 26 (blue arrows) is a minor component of the sample.

Based on SEM inages it appears that the porosity in sample 2 (7,128.6 ft.) is more uniformally distributed than porosity in sample 1 (7073.9 ft.). The SEM photos reveal that there is a volume of porosity that cannot be detected by thin-section analysis. Porosity not visible with light microscopy plays a role in fluid storage and fluid flow properties. Small pore throats only visible under the SEM may or may not contribute to the effective permeability of the reservoir to water or oil.

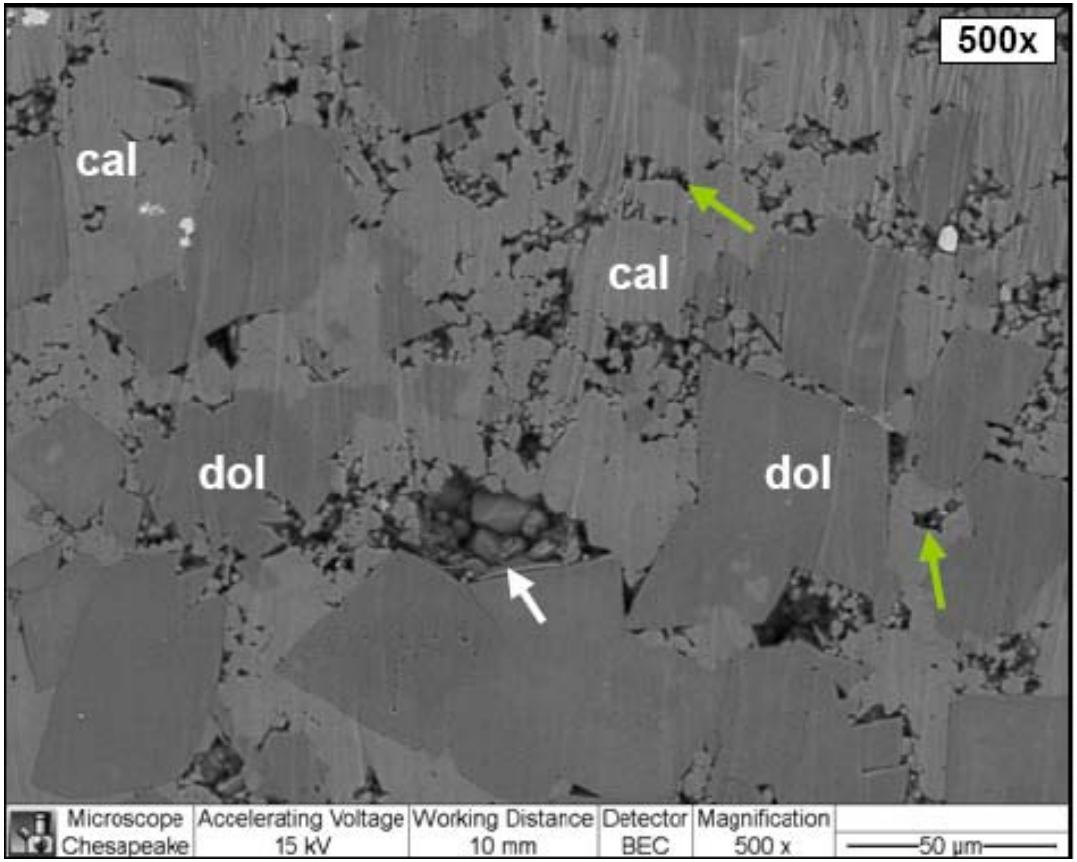

Figure 24. Scanning electron microscope image at 7128.6 ft. at 500x. Dolomite (dol) and calcite (cal) make up the dolomitized skeletal wackestone. Intercrystalline porosity is shown by the green arrows. The white arrow indicates a vuggy pore. Image taken by Rick Urash at Chesapeake Energy Reservoir Technology Center.

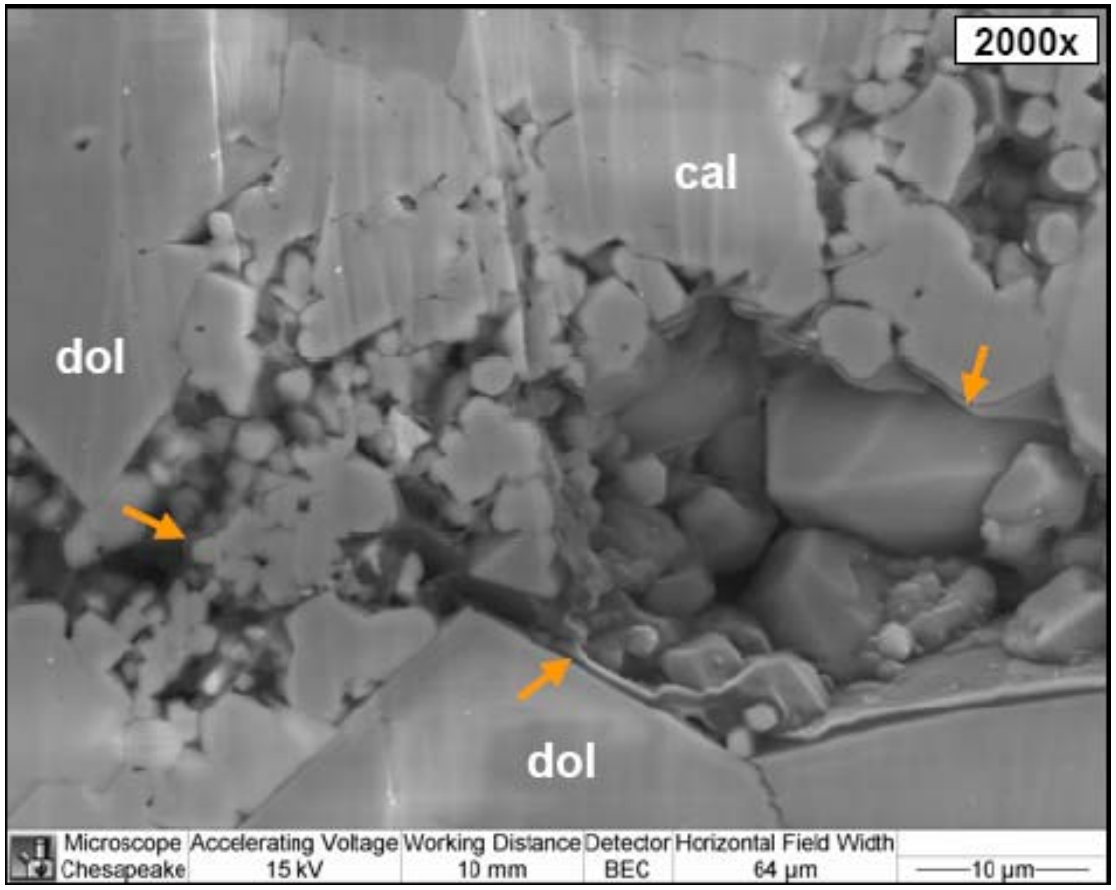

Figure 25. Scanning electron microscope image at 7,128.6 ft. at 2,000x. Dolomite (dol) and calcite (cal) make up the dolomitized skeletal wackestone. Calcite cement (orange arrows) lines the pores. Image taken by Rick Urash at Chesapeake Energy Reservoir Technology Center.

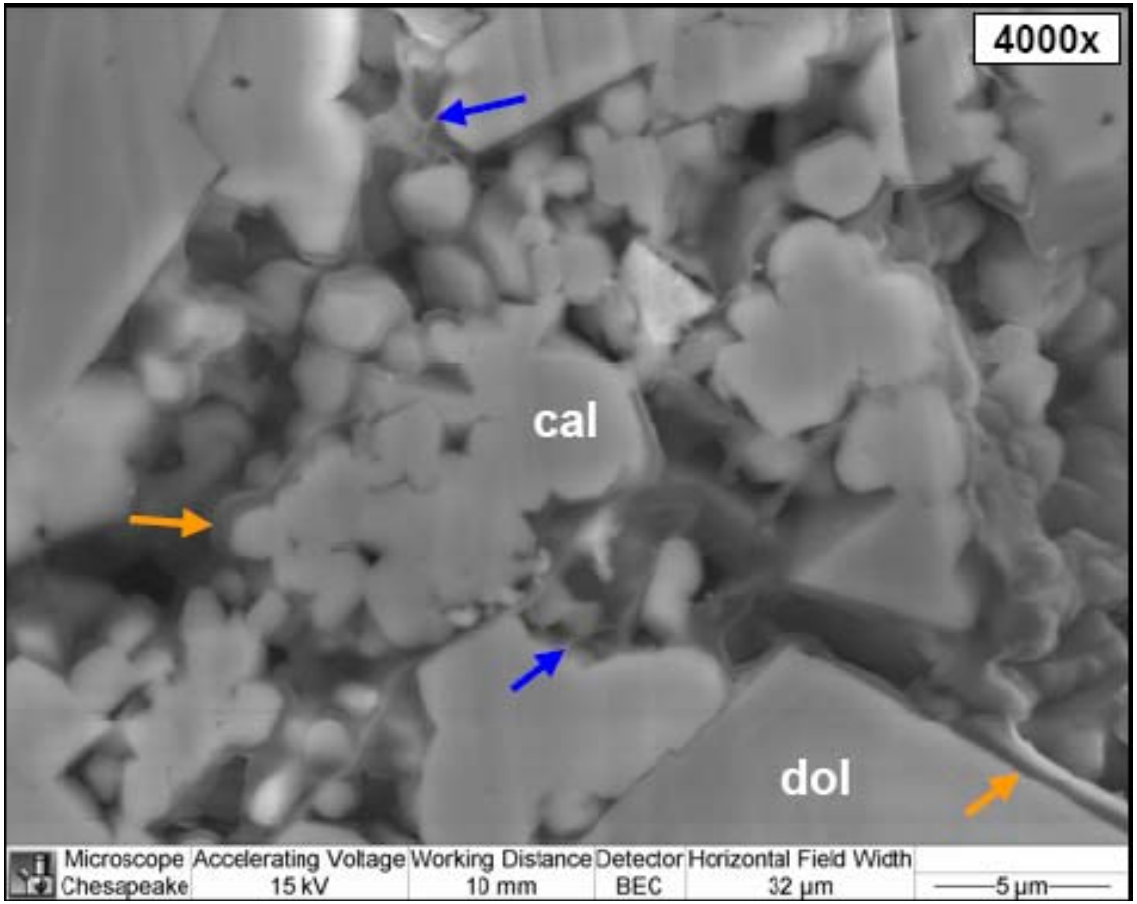

Figure 26. Scanning electron microscope image at 7,128.6 ft. at 4,000x. Dolomite (dol) and calcite (cal) make up the dolomitized skeletal wackestone. Calcite cement (orange arrows) lines the pores. Authigenic illite (blue arrows) partially fills the pore space. Image taken by Rick Urash at Chesapeake Energy Reservoir Technology Center.

Modern Wire-Line Log Analysis

Nineteen modern wireline-logs, whose locations are shown in Figure 27 were evaluated using techniques developed by George G. Asquith (1985) in his book, "Handbook of Log Evaluation Techniques for Carbonate Reservoirs." Bulk Volume Water (BVW) is the product of water saturation (Sw) multiplied by porosity. Water saturation was calculated using the Archie equation. BVW is a function of grain size, pore size, and the type of carbonate porosity (Asquith, 1985). Porosity and resistivity input from wire-line log data was used to calculate water saturation using the standard Archie equation. Core, thin section, and SEM analysis of the West Edmond SWD 1-24 was used to tie wire-line log data calculations to reservoir properties derived from the West Edmond SWD 1-24 analysis. The goal is to correlate reservoir properties from the West Edmond SWD 1-24 to the rest of the West Edmond Field.

The Frisco Formation and pre-Frisco carbonates can be divided into three wire-line log calculated petrophysical units. The petrophysical units are defined as

petrophysical facies A (pink), petrophysical facies B (green), and petrophysical facies C (tan), which can be viewed in Figure 28. Each petrophysical unit has a unique lithology, depositional environment, and dominant pore type; thus each petrophysical unit has its own unique fluid flow properties. The core derived porosity and permeability in Figure28 are posted to the right of the log for the West Edmond SWD 1-24.

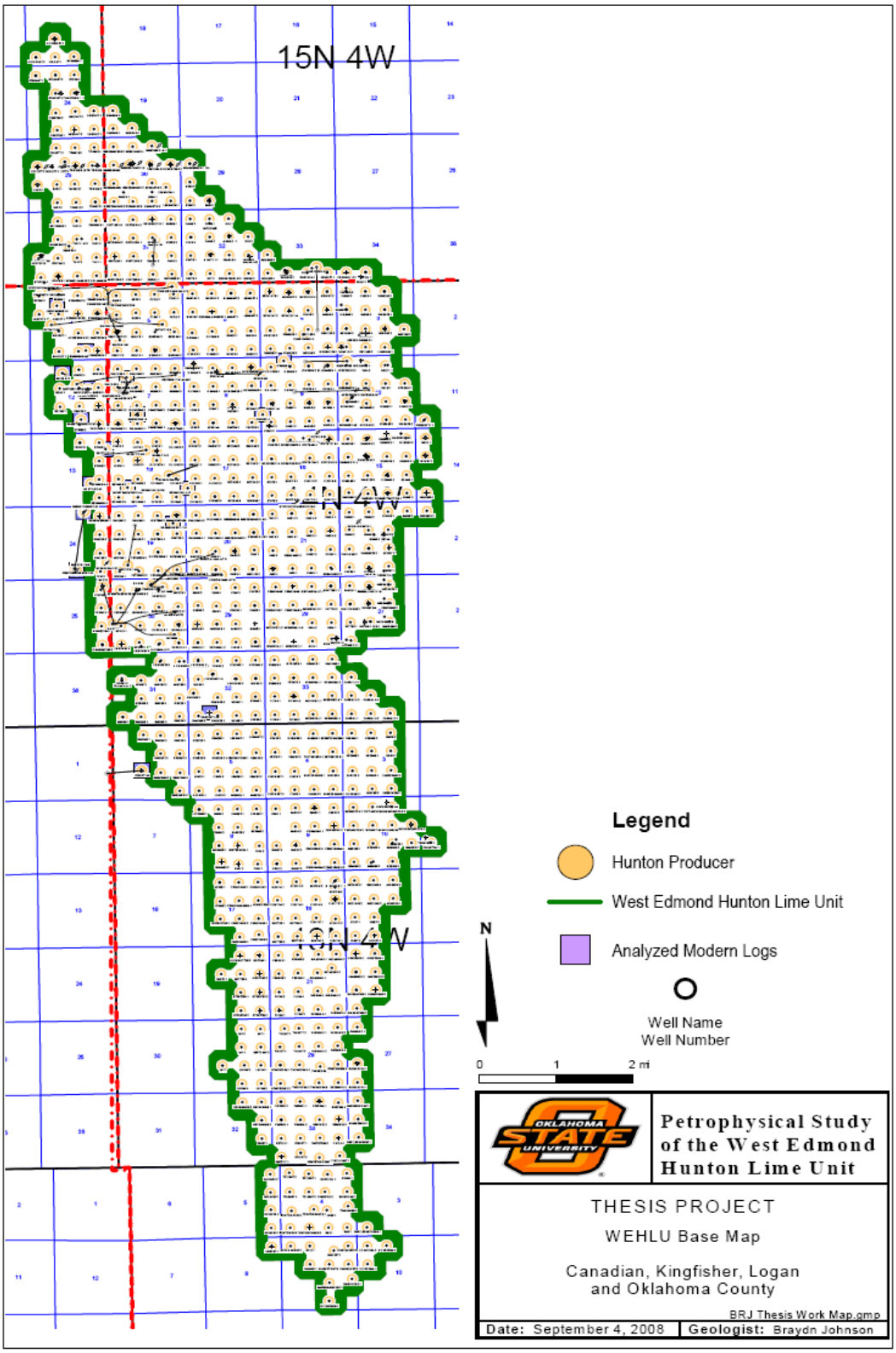

Figure 27- Base Map of West Edmond Field. The nineteen modern logs analyzed in this study are indicated by purple squares.

Figure 28 shows the stacking pattern of wire-line-log-calculated petrophysical units compared to the log responses, and lab calculated porosity and permeability for the West Edmond SWD 1-24. Wire-line log response and permeability measurements corroborate the findings of (Littlefield, 1947) that the vertical distribution of the porosity is far from uniform.

Petrophysical Facies

Petrophysical facies A consists of skeletal grainstones and packstones. The best reservoir rocks in the Hunton analyzed by Kopaska-Merkel (1989) are crinoidal grainstones and packstones. The dominant porosity type is intraparticle porosity. Core-derived porosity ranges from 1.5%-9.5%. Core-derived permeability ranges from 0.5md-5md. The pagoda diagram to the left of the log in Figure 28 shows that petrophysical facies A is primarily composed of calcite (blue). The BVW calculated in petrophysical facies A ranges from 0.0141-0.0283. Carbonate porosity types calculated from (Asquith, 1985) range from vuggy, vuggy and intercrystalline/intergranular, to intercrystalline/intergranular. Grain size determination using the classification of (Fertl, 1978) ranges from N/A (to large for scale), coarse (1.0mm-0.5mm), to medium (0.5mm-0.25mm).

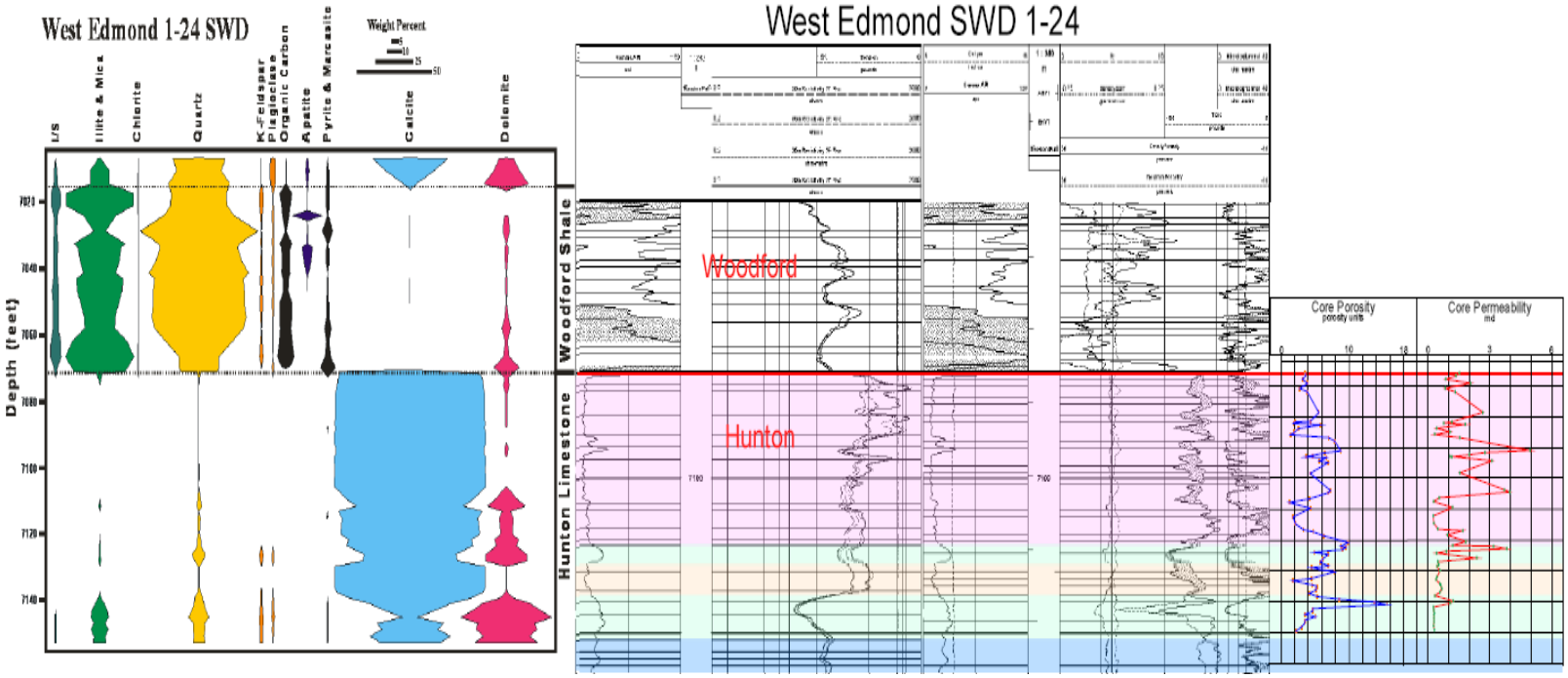

Figure 28. Pagoda diagram,"Bois d'Arc" petrophysical units superimposed on West Edmond SWD 1-24 wire-line logs, and core-derived porosity and permeability for the cored Hunton Group in the West Edmond SWD 1-24.

The range in grain size is a function of the early syntaxial calcite overgrowth on echinoderm fragments that increase the size of the initial grain.

Petrophysical facies B consists of dolomitized skeletal wackestones. The dominant porosity is intercrystalline porosity. There are various degrees of dolomitiziation within petrophysical facies B. Higher porosities and permeabilities are associated with zones with the highest percentage of dolomitization. The correlation between the percentage of dolomite (pink), core derived porosity, and core derived permeability can be seen in Figure 28. Core-derived porosity ranges from 2%-15%. Core-derived permeability ranges from 0.2md-3.7md. Petrophysical facies B has higher dolomite content than any of the other petrophysical facies. The BVW calculated in petrophysical facies B ranges from 0.0258-0.0707. Carbonate porosity types (Asquith, 1985) range from intercrystalline/intergranular, to chalky. The chalky classification is due to the sucrosic nature of the dolomite and the fine crystalline carbonate mud within the wackestone. Grain size (Fertl, 1978) ranges from medium (0.5mm-0.25mm), fine (0.25mm-0.125mm), very fine (0.125mm-0.0625mm), to silt (<0.0625mm).

Petrophysical facies C consists of skeletal oolitic grainstones. The dominant porosity is moldic. Core-derived porosity ranges from 2%-8%. Core-derived permeability ranges from 0.3md-0.6md. The pagoda diagram illustrates that petrophysical facies C is primarily composed of calcite. The BVW calculated in petrophysical facies C ranges from 0.02-0.023. Porosity (Asquith, 1985) ranges from vuggy, to vuggy and intercrystalline/intergranular. Grain size (Fertl, 1978) ranges from N/A (to large for scale) to coarse (1.0mm-0.5mm). The large grain size is a function of early syntaxial calcite

overgrowth on ooids that is similar to early syntaxial calcite overgrowths on echinoderm fragments in petrophysical facies A.

Fracture Analysis

Fracture data was collected from the West Edmond SWD 1-24 core by the Reservoir Technology Center at Chesapeake Energy. Fractures are approximately oriented east-west. Structural movements associated with the Oklahoma City Uplift were probably of sufficient magnitude to form fractures in the Hunton Group before, after, and possibly during the time the Hunton was exposed to subaerial weathering.

Lateral Extent of Petrophysical Units

Four cross sections were constructed using 16 of the 19 modern logs suites. Two cross-sections (A-A^1, B-B^1) are dip sections and 2 cross-sections (C-C^1, D-D^1) are strike sections seen in Figure 29. Each cross-section has been overlain with the 3 petrophysical

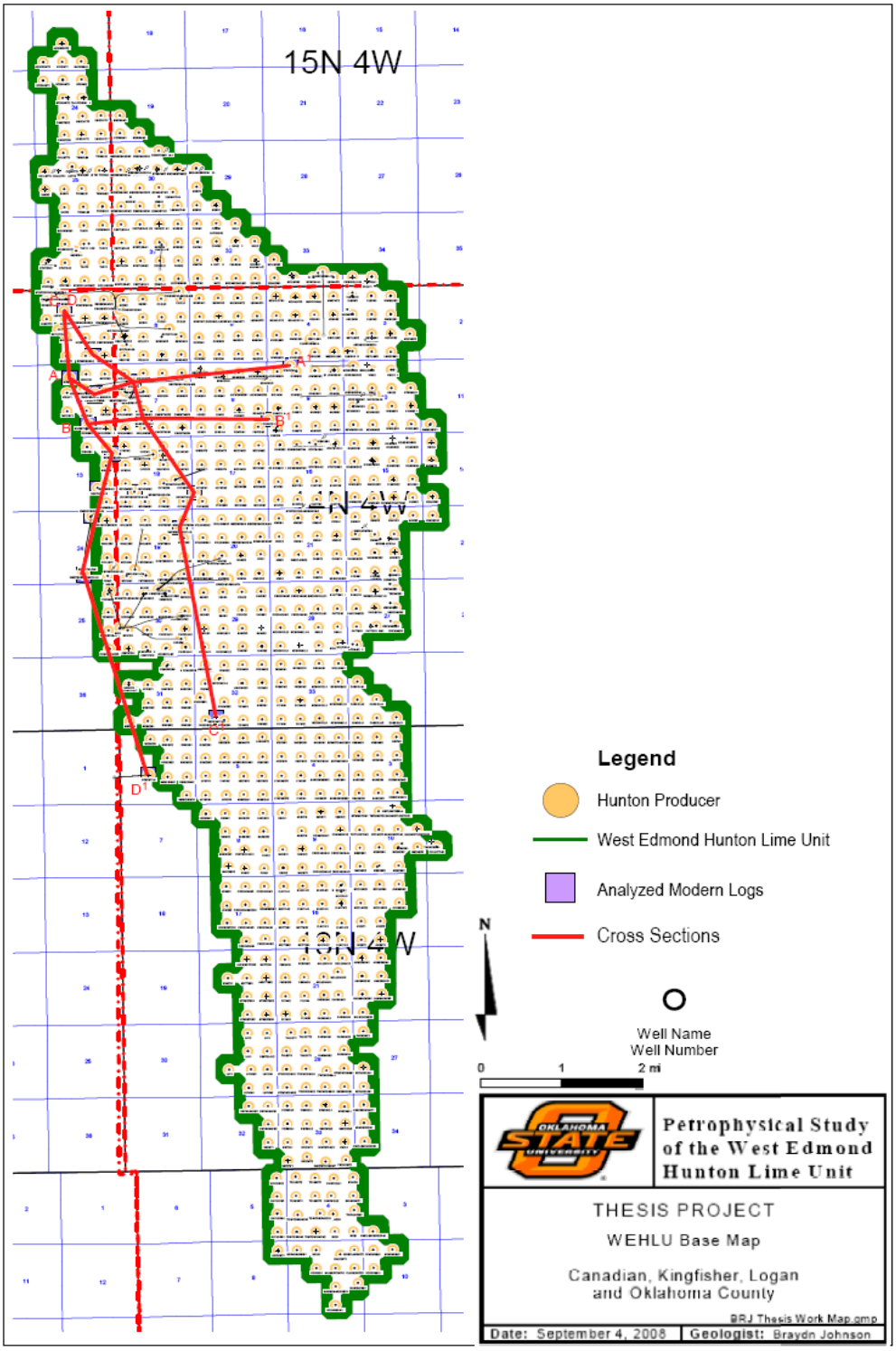

Figure 29. Location of stratigraphic cross-sections (red lines) for the West Edmond Field.

units previously described (petrophysical facies A, petrophysical facies B, petrophysical facies C). The cross-sections were combined to predict the spatial distribution of each petrophysical unit and make inferences about fluid flow paths within the Hunton interval.

Cross-section A-A^1 is the northernmost west to east cross-section and consists of the following wells: Mr. Ed 1-12 (Sec.12, T.14N., R.5W.), Chupa 1-12 SWD (Sec.12, T.14N., R.5W.), Willy 1-7 (Sec.7, T.14N.,R.4W.), and O'Brien 1-9 (Sec.9,T.14N.,R.4W.) (Figure 30). The Mr. Ed 1-12 has 12 feet of petrophysical facies B at the base, overlain by 18 feet petrophysical facies C, overlain by 10 feet of petrophysical facies B, and capped by 28 petrophysical facies A. The Chupa 1-12 SWD contains 10 feet of petrophysical facies B at the base, overlain by 20 feet of petrophysical facies C, and is capped by 36 feet of petrophysical facies A. The Willy 1-7 has 21 feet of petrophysical B at the base, overlain by 16 feet of petrophysical facies C, overlain by 6 feet of petrophysical facies B, and capped by 24 feet of petrophysical facies A. The O'Brien 1-9 has 8 feet of petrophysical facies B at the base, overlain by 10 feet of petrophysical facies C, overlain by 17 feet of petrophysical facies A, and capped by 3 feet of petrophysical facies B. The entire thickness of the targeted zone decreases up-dip. The upper petrophysical faces B pinches out in the Chupa 1-12 SWD and the O'Brien 1-9. Petrophysical facies A caps the target zone for each well except the O'Brien 1-9. Petrophysical facies A becomes thicker when the upper petrophysical facies B pinches out. The thickness of petrophysical facies A, B, and C thin as they extend up-dip.

Cross-section B-B^1 is the southernmost west to east cross-section and consists of the following wells: Majesty's Crown 2-12 (Sec.12, T.14N., R.5W.), Damogram 1-7 (Sec.7, T.14N., R.4W.), and Caracol 1 (Sec.9, T.14N., R.5W.) (Figure 31). The

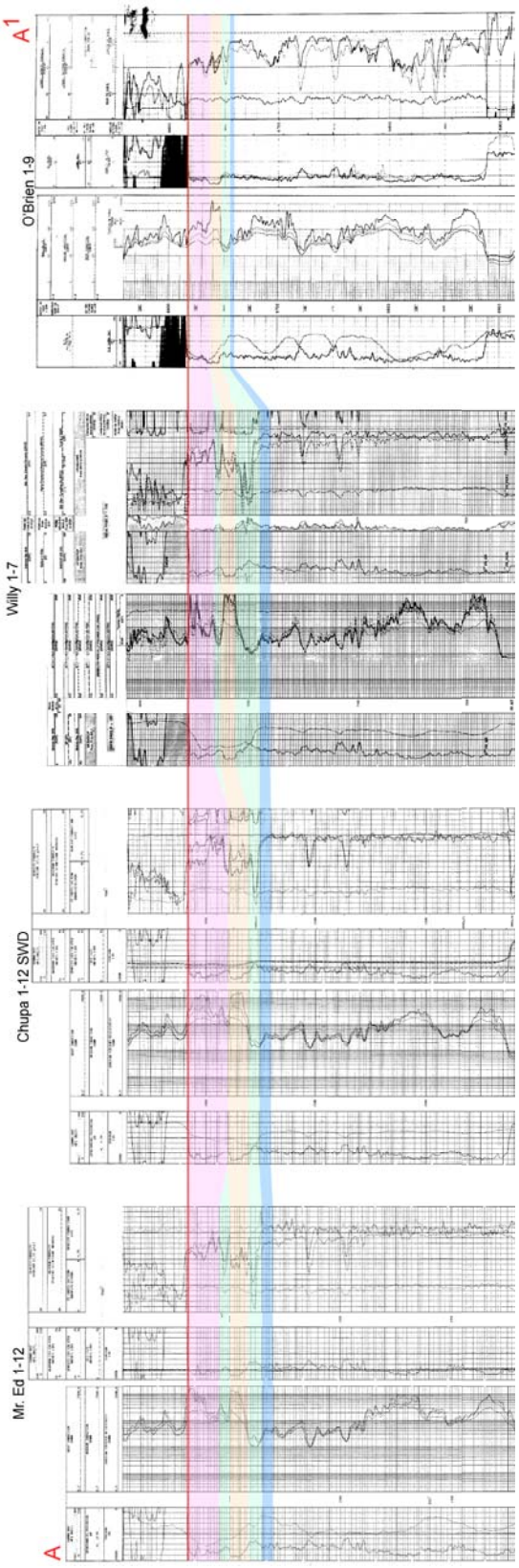

Figure 30. Stratigraphic cross-section A-A^{1}. Datum is the base of the Woodford Shale. Pink represents facies A, facies B is shown by green, and facies C is tan.

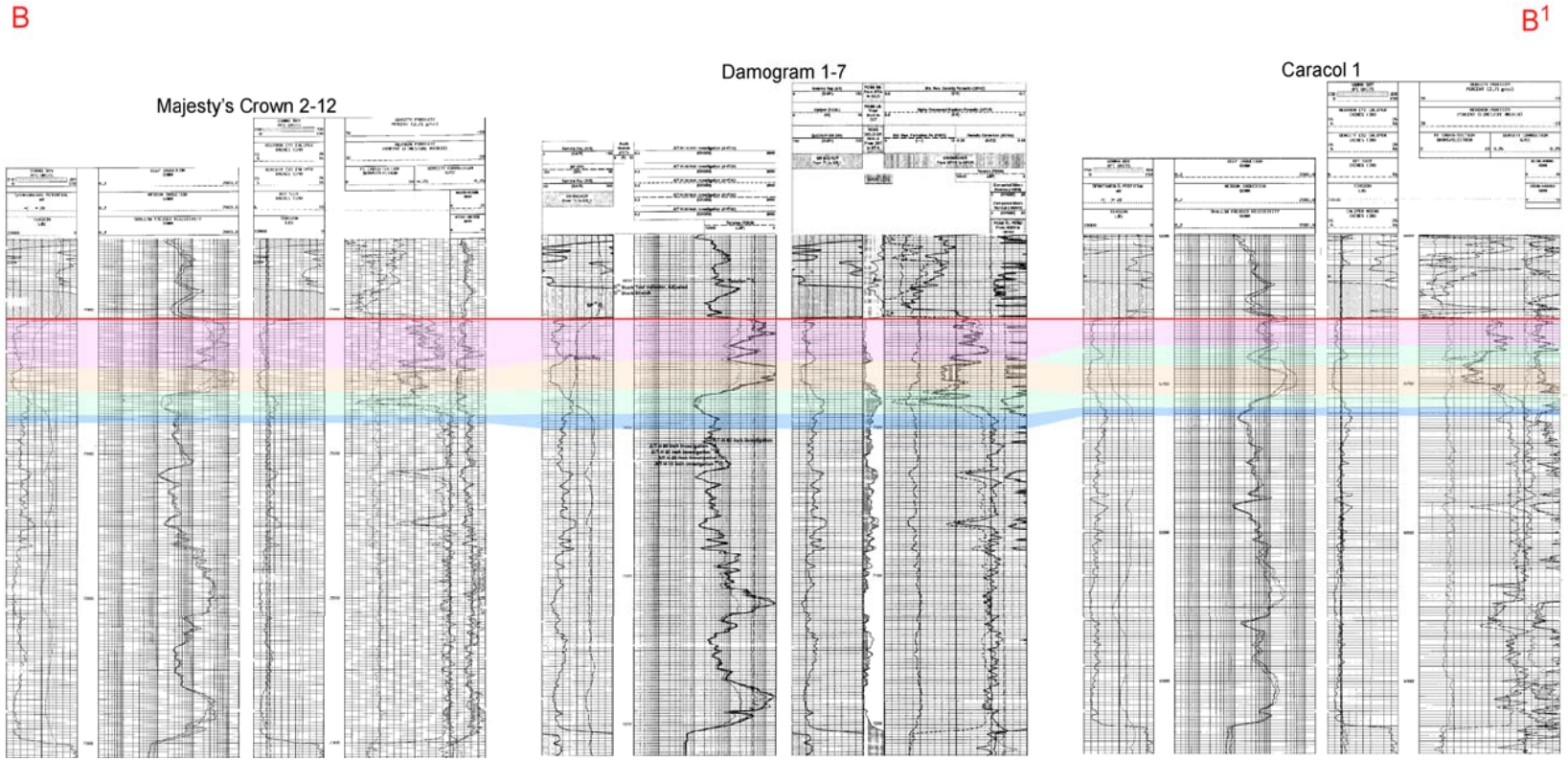

Figure 31. Stratigraphic cross-section B-B[1]. Datum is the base of the Woodford Shale. Pink represents facies A, facies B is green, and facies C is tan.

Majesty's Crown 2-12 has 16 feet of petrophysical facies B at the base, overlain by 17 feet of petrophysical facies C, and is capped by 34 feet of petrophysical facies A. The Damogram 1-7 has 17 feet of petrophysical facies B at the base, overlain by 19 feet of petrophysical facies C, and capped by 28 feet of petrophysical facies A. The Caracol 1 has 16 feet of petrophysical facies B at the base, overlain by 20 feet of petrophysical facies C, and capped by 28 feet of petrophysical facies A. The upper petrophysical facies B is not present in Majesty's Crown 2-12 or Damogram 1-7. The target section in cross-section B-B^1 does not thin as compared to cross section A-A^1.

Cross-section C-C^1 is the easternmost north to south cross-section and consists of the following wells: Lucky Horse 1-1 (Sec.1, T.14N., R.5W.), Lucky Horse 2-1 (Sec.1, T.14N., R.5W.), Willy 1-7 (Sec.7, T.14N., R.4W.), Damogram 1-7 (Sec.7, T.14N., R.4W.), Spunky Gal 1-17 (Sec., T.14N., R.5W.), Unbridled Boy 1-19 (Sec.19, T.14N., R.4W.), and Recount 1-32 (Sec.32, T.14N., R.5W.) (Figure 32). The Lucky Horse 1-1 has 18 feet of petrophysical facies B at the base, overlain by 14 feet of petrophysical facies C, overlain by 8 feet of petrophysical facies b, and capped by 28 feet of petrophysical facies A. The Lucky Horse 2-1 contains 18 feet of petrophysical facies B at the base, overlain by 14 feet of petrophysical facies C, overlain by 10 feet of petrophysical facies B, and capped by 24 feet of petrophysical facies A. The Willy 1-7 has 21 feet of petrophysical B at the base, overlain by 16 feet of petrophysical facies C, overlain by 6 feet of petrophysical facies B, and capped by 24 feet of petrophysical facies A. The O'Brien 1-9 has 8 feet of petrophysical facies B at the base, overlain by 10 feet of petrophysical facies C, overlain by 17 feet of petrophysical facies A, and capped by 3 feet of petrophysical facies B. The Damogram 1-7 has 17 feet of petrophysical facies B at the

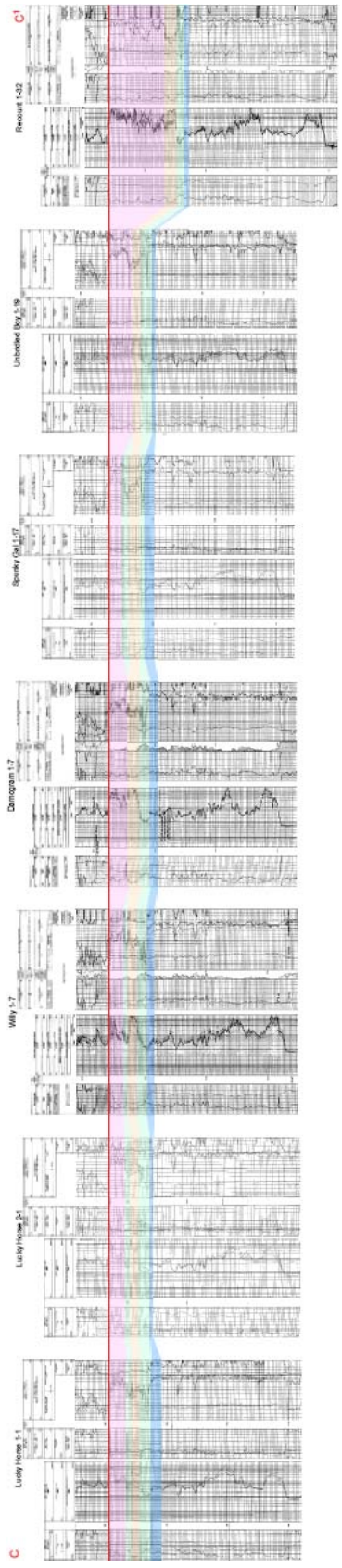

Figure 32. Stratigraphic cross-section C-C[1]. Datum is the base of the Woodford Shale. Pink represents facies A, green facies B, and tan facies C.

base, overlain by 19 feet of petrophysical facies C, and capped by 28 feet of petrophysical facies A. The Spunky Gal 1-17 has 8 feet of petrophysical facies B at the base, overlain by 18 feet of petrophysical facies C, overlain by 10 feet of petrophysical facies B, and capped by 21 feet if petrophysical facies A. The Unbridled Boy 1-19 has 18 feet of petrophysical facies B at the base, overlain by 14 feet of petrophysical facies C, and capped by 37 feet of petrophysical facies A. The Recount 1-32 has 12 feet of petrophysical facies B at the base, overlain by 20 feet of petrophysical facies C, capped by 92 feet of petrophyscial facies A. Upper petrophysical facies B is absent in the Damogram 1-7, Unbridled Boy 1-19, and Recount 1-32. The Unbridled Boy 1-19 and Recount 1-32 show the thickening of capping petrophysical facies A.

Cross-section D-D^{1} is the western most north to south cross-section and consists of the following wells: Lucky Horse 1-1 (Sec.1, T.14N., R.5W.), Mr. Ed 1-12 (Sec.12, T.14N., R.5W.), Majesty's Crown 2-12 (Sec.12, T.14N., R.5W.), D.G. Style 1-13 (Sec. 13, T.14N., R. 5W.), Marilyn 1-24H (Sec. 24, T.14N., R.5W.), West Edmond SWD 1-24 (Sec. 24, T.14N., R.5W.) , and Specht 1-6 (Sec. 6, T.14N., R.4W.) (Figure 33). The Lucky Horse 1-1 has 18 feet of petrophysical facies B at the base, overlain by 14 feet of petrophysical facies C, overlain by 8 feet of petrophysical facies b, and capped by 28 feet of petrophysical facies A. Mr. Ed 1-12 has 12 feet of petrophysical facies B at the base, overlain by 18 feet petrophysical facies C, overlain by 10 feet of petrophysical facies B, and capped by 28 petrophysical facies A. Majesty's Crown 2-12 has 16 feet of petrophysical facies B at the base, overlain by 17 feet of petrophysical facies C, and is capped by 34 feet of petrophysical facies A. D.G. Style 1-13 has 14 feet of petrophysical facies B, overlain by 18 feet of petrophysical facies C, and is capped by 38 feet if

Figure 33. Stratigraphic cross-section A-A[1]. Datum is the base of the Woodford Shale. Pink represents facies A, green facies B, and tan facies C. The Marilyn 1-24 H is a deviated well bore, thus, the Hunton Group appears thicker.

An increase in thickness of each zone seemingly gives the wire-line logging tools a higher resolution. The stacking pattern of the petrophysical facies within the Marilyn 1-24 H appears to be higher resolution compared to the analyzed vertical well bores. Marilyn 1-24 H has 22 feet of petrophysical facies B at the base, overlain by 24 feet of petrophysical facies C, 16 feet of petrophysical facies B, 62 feet of petrophysical facies A, 5 feet of petrophysical facies B, 14 feet of petrophysical facies A, 8 feet of petrophysical facies B, and capped by 18 feet of petrophysical facies A. West Edmond SWD 1-24 has 14 feet of petrophysical facies B at the base, overlain by 10 feet of petrophysical facies C, overlain by 6 feet of petrophysical facies B, and capped by 56 feet of petrophysical facies A. Specht 1-6 has 14 feet of petrophysical facies B at the base, overlain by 12 feet of petrophysical facies C, capped by 106 feet of petrophysical facies A. Upper petrophysical facies B pinches out in the Majesty's Crown 2-12, D.G. Style 2-13, and Specht 1-6. Petrophysical facies A thickens towards the south at the expense of petrophysical facies B and petrophysical facies C.

Correlation of Petrophysical Facies to Depositional Facies

The connection between the petrophysical facies and depositional environment is important to understanding the genesis of reservoirs. Figure 34 demonstrates the correlation between the depositional facies and petrophysical facies.

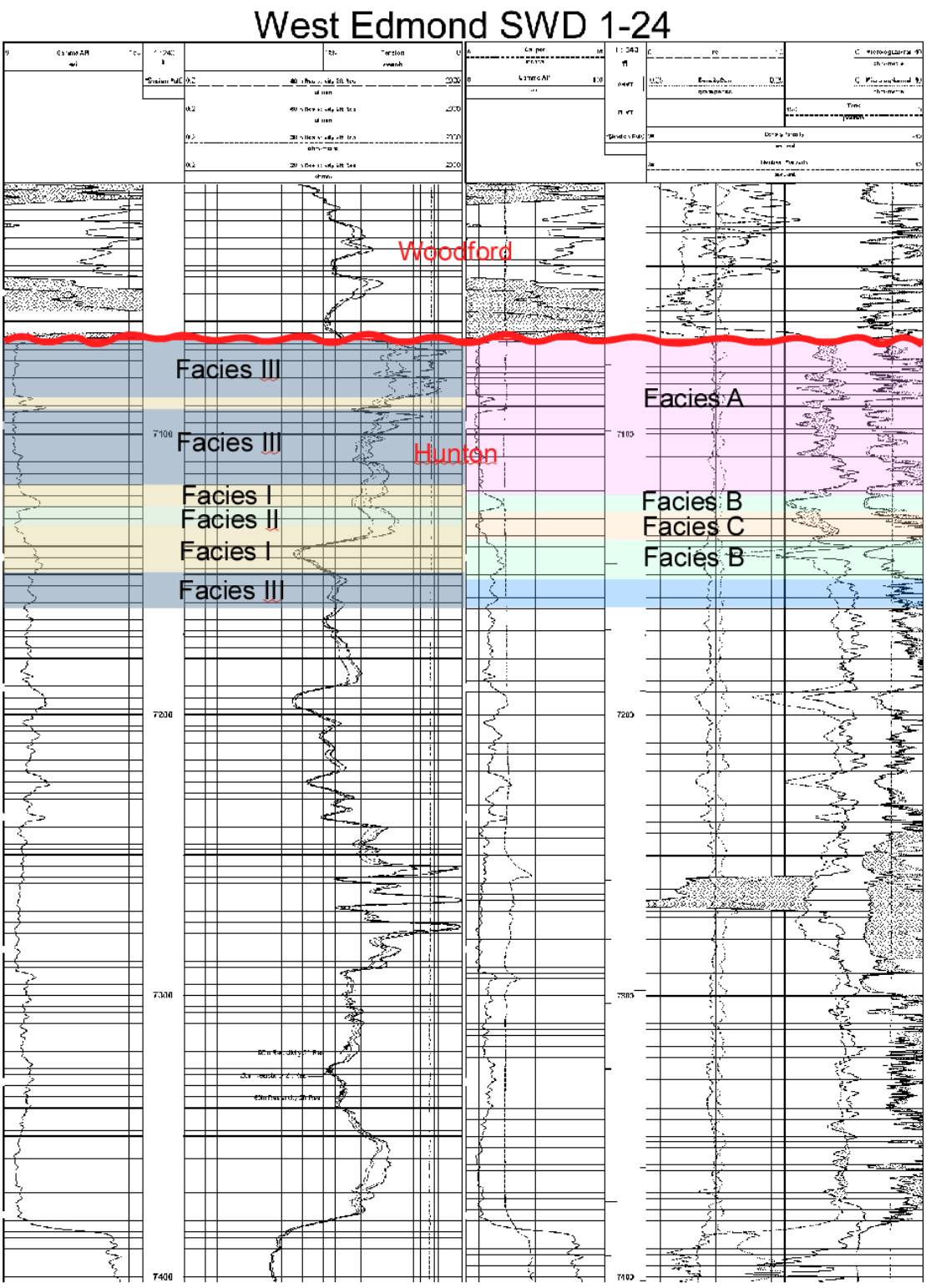

Figure 34. Hunton depositional facies and “Bois d’Arc” petrophysical facies superimposed on West Edmond SWD 1-24 wire-line logs.

Grain rich, cleaner carbonates such as the Frisco Limestone and higher energy upper subtidal carbonates in the pre-Frisco section comprise petrophysical facies A. These rocks are dominated by intraparticle porosity and solution-enlarged fractures. As a result, they have higher permeability and were efficiently drained during the early development of the West Edmond Field.

Dolomitized skeletal wackestones of the pre-Frisco section contain extensive matrix porosity and fewer fractures. The diffuse porosity and lower permeability of this interval was less-efficiently produced by the primary and secondary production stages. These wackestones correspond to facies I in the depositional model and petrophysical facies B.

Oolitic grainstones of the pre-Frisco section contain moldic porosity and fewer fractures. This oomoldic porosity is associated with lower-permeabilities. As a result, these rocks were less-efficiently produced by primary and secondary production stages. The oolitic grainstones correspond to facies II in the depositional model and petrophysical facies C.

Detailed mapping of the petrophysical facies can be used to define inadequately drained parts of the reservoir. Further studies of the West Edmond Field can utilize the petrophsyical facies previously described to evaluate the Frisco Formation and pre-Frisco carbonates for additional oil and gas production.

CHAPTER VI

CONCLUSIONS

The collection and analysis of data from the West Edmond Field allows for the following interpretations of the Hunton Group Carbonates:

1. A shallow ramp setting with carbonate mounds explains the depositional facies evident in the West Edmond SWD 1-24 core. The stacking of the facies in interpreted as being the result of relative sea level changes, and the related shift in shoreline. The interpretation of this vertical facies succession is complicated by possible subaerial exposure and erosion.

2. Detailed examination of samples from the cored interval using thin section petrography, scanning electron microscopy, porosity, permeability, and wire-line logs supports correlating these findings to the establishing the following petrophysical facies.

A. Petrophysical facies A consists of skeletal grainstones and packstones. The dominant porosity type is intraparticle porosity. Core-derived porosity ranges from 1.5%-9.5%. Core-derived permeability ranges from 0.5md-5md. Carbonate porosity types range from vuggy, vuggy and intercrystalline/intergranular, to intercrystalline/intergranular. Grain size ranges coarse (1.0mm-0.5mm), to medium (0.5mm-0.25mm).

B. Petrophysical facies B consists of dolomitized skeletal wackestones. The dominant porosity is intercrystalline porosity. There are various degrees of dolomitiziation within petrophysical facies B. Higher porosities and permeabilities are associated with zones with the highest percentage of dolomitization. Core-derived porosity ranges from 2%-15%. Core-derived permeability ranges from 0.2md-3.7md. Petrophysical facies B has higher dolomite content than any of the other petrophysical facies. Carbonate porosity types range from intercrystalline/intergranular, to chalky. The chalky classification is due to the sucrosic nature of the dolomite and the fine crystalline carbonate mud within the wackestone. Grain size ranges from medium (0.5mm-0.25mm), fine (0.25mm-0.125mm), very fine (0.125mm-0.0625mm), to silt (<0.0625mm).

C. Petrophysical facies C consists of skeletal oolitic grainstones. The dominant porosity is moldic. Core-derived porosity ranges from 2%-8%. Core-derived permeability ranges from 0.3md-0.6md. Porosity ranges from vuggy, to vuggy and intercrystalline/intergranular. Grain size ranges is coarse (1.0mm-0.5mm). The large grain size is a function of early syntaxial calcite overgrowth on ooids.

3. Petrophysical facies have varying permeabilities. The vertical stacking pattern of petrophysical facies effects the production. High-permeability zones, such as petrophysical facies A, were depleted of hydrocarbons and channeled water during secondary recovery efforts. Petrophysical facies of lower-permeabilities are not adequately produced. High-permeablity zones (facies A) were depeleted of hydrocarbons, whereas low-permeability zones (facies B and facies C) are still capable of producing economic volumes of oil and gas.

REFERENCES

Adler, Frank J. "Anadarko Basin and Central Oklahoma Area: Region 7." Future Petroleum Provinces of the United States-- Their Geology and Potential 2 (1971): 1061-070.

Al-Shaieb, Zuhair, Jim Puckette, and Paul Blubaugh. "The Hunton Group: Sequence Stratigraphy, Facies, Dolomitization, and Karstification." Oklahoma Geological Survey Special Publication 2000-2 (2000): 39-50.

Amsden, T. W., and J. E. Barrick. "Late Ordovician Through Early Devonian Annotated Correlation Chart and Brachioppod Range Charts for the Southern Mid-Continent Region, U.S.A., with a Discussion of Silurian and Devonian Conodont Faunas." Oklahoma Geologic Survey Bulletin 143 (1988).

Amsden, T. W., and T. L. Rowland. "Silurian and Lower Devonian (Hunton) Oil-and-Gas Producing Formations." AAPG Bulletin 55 (1971): 104-09.

Amsden, T. W. "Hunton Group (Late Ordovician, Silurian , and Early Devonian) in the Arkoma Basin of Oklahoma." Oklahoma Geological Survey Bulletin 129 (1980).

Amsden, T. W. "Hunton Group (Late Ordovician, Silurian, and Early Devonian) in the Arkoma Basin of Oklahoma." Oklahoma Geological Survey Bulletin 121 (1975).

Amsden, T. W. "Hunton Stratigraph, Part VI of Stratigraphy and Paleontology of the Hunton Group in the Arbuckle Mountains Region." Oklahoma Geologic Survey Bulletin 84 (1960).

Amsden, T. W. "Part VI of Hunton Stratigraphy." Oklahoma Geological Survey Bulletin 84 (1959).

Amsden, T. W. "Silurian and Devonian Strata in Oklahoma." Tulsa Geological Society Digest 35 (1967): 25-34.

Amsden, T. W. "Silurian and Early Devonian Carbonate Rocks of Oklahoma." AAPG Buletin 46 (1962): 1502-519.

Amsden, T. W. "Stratigraphy and Paleontology of the Hunton Group in the Arbuckle Mountains Region." Oklahoma Geological Survey Bulletin 78 (1958).

Amsden, T. W. "Stratigraphy of the Frisco and Sallisaw Fromations (Devonian) of Oklahoma." Oklahoma Geological Survey Bulletin 90 (1961).

Archie, G. E. "Classification of Carbonate Reservoir Rocks and Petrophysical Considerations." AAPG Bulletin 2nd ser. 36 (1952): 278-98.

Asquith, George B. Handbook of Log Evaluation Techniques for Carbonate Reservoirs. Tulsa, OK: The American Association of Petroleum Geologists, 1985. 1-47.

Bathurst, Robin G. Carbonate Sediments and Their Diagenesis. 2nd ed. New York, NY: Elsevier Scientific Company, 1975. 1-658.

Budd, David A. "The Relative Roles of Compaction and Early Cementation in the Destruction of Permeability in Carbonate Grainstones: A Case Study from the Paleogene of West-Central Florida, U.S.A." Journal of Sedimentary Research 1st ser. 72 (2002): 116-28.

Choquette, P. W., and L. C. Pray. "Geologic Nomenclature and Classification of Porosity in Sedimentary Carbonates." AAPG Bulletin 2nd ser. 54 (1970): 207-50.

Dunham, R. J. "Classification of Carbonate Rocks According to Depositional Texture." AAPG Memoir No. 1 (1961): 108-21.

Elkins, Lincoln F. "Internal Anatomy of a Tight, Fractured Hunton Lime Reservoir." SPE-AIME (1969): 221-32.

Fritz, Richard D., and Patrick L. Medlock. "Sequence Stratigraphy of the Hunton Group as Defined by Core, Outcrop, and Log Data." Bulletin Houston Geological Society (1994): 29-58.

Hill, Gerhard W. "The Anadarko Basin: A Model for Regional Petroleum Accumulations." Technical Proceedings of the 1981 AAPG Mid-Continent Regional Meeting (1984): 1-23.

Hobson, G. D. "Carbonate Deposits and Oil Accumulations." Oil Field Development Techniques: Proceedings of the Daqing International Meeting 28 (1982): 159-74.

Hoffman, P., J. F. Dewey, and K. Burke. "Aulacogens and Their Genetic Relation to Geosynclines, with a Proterozoic Example from Great Slave Lake, Canada." SEPM Special Publication 12 (1974): 38-55.

Houseknecht, David W. "Thin Section Analysis." Development Geology Reference Manual 10 (1992): 233-36.

Jennings, James W., and Jerry F. Lucia. "Predicting Permeability From Well Logs in Carbonates with A Link to Geology for Interwell Permeability Mapping." SPE Bulletin (2003): 215-26.

Johnson, K. S., ed. "Hunton Group Core Workshop and Field Trip." Oklahoma Geologic Survey Special Publication 93-4: 161-80.

Kopaska-Merkel, David C., and Gerald M. Friedman. "Petrofacies Analysis of Carbonate Rocks: Example from Lower Paleozoic Hunton Group of Oklahoma and Texas." AAPG Bulletin 1st ser. 73 (1989): 1289-306.

Littlefield, Max. "Comments on Limestone Porosity." Tulsa Geological Society Digest 8 (1939).

Littlefield, Max, L. L. Gray, and A. C. Godbold. "Reservoir Study of the West Edmond Hunton Pool, Oklahoma." SPE AIME 174th ser. (1948): 131-55.

Lonoy, Arve. "Making Sense of Carbonate Pore Systems." AAPG Bulletin 9th ser. 90 (2006): 1381-405.

Lucia, J. F. Carbonate Reservoir Characterization. Berlin: Springer-Verlag, 1999. 1-226.

Lucia, J. F. "Petrophysical Parameters estimated from Visual Descriptions of Carbonate Rocks: A Field Classification of Carbonate Pore Space." Journal of Petroleum Technology 216 (1983): 221-24.

Lucia, J. F., W. J. Jennings, and C. S. Ruppel. "South Wasson Clear Fork Reservoir Modeling: The Rock Fabric Method for Constructing Flow Layers For Fluid Simulation." AAPG Hedberg Research Conference (2004).

Lucia, Jerry F. "Diagenesis of a Crinoidal Sediment." Journal of Sedimentary Petrology 4th ser. 32 (1962): 848-65.

Lucia, Jerry F. "Rock-Fabric/Petrophysical Classification of Carbonate Pore Space for Reservoir Characterization." AAPG Bulletin 9th ser. 79 (1995): 1275-300.

Mateu, Esteban. Carbonate Field Databas. Vers. Phase Four. May 2002. Carbonates International.

Mazzullo, S. J. Sedimentary Processes in Ancient Carbonates. Comp. John M. Cys. Tulsa, OK: Society of Economic Paleontologists and Mineralogists, 1978. 1-235.

Mazzullo, S. J. Stratigraphic Traps in Carbonate Rocks. Ann Arbor, MI: Edwards Brothers, Inc., 1980. 1-217.

McGee, D. A., and H. D. Jenkins. "West Edmond Field, Central Oklahoma." AAPG Bulletin 1797th ser. 30 (1946).

Medlock, P. L. "Depositional Environment and Diagenetic History of the Frisco and Henryhouse Formations in Central Oklahoma." Thesis. 1-146.

Medlock, Patrick L. "Depositional Model and Diagnentic History of Frisco Formation (Lower Devonian) in Central Oklahoma: ABSTRACT." AAPG Bulletin 71 (1987): 994-94.

Moore, Clyde H. Carbonate Reservoirs : Porosity Evolution and Diagenesis in a Sequence Stratigraphic Framework. St. Louis: Elsevier Science, 2001. 1-444.

Northcutt, Robert A. "History of Hunton Oil and Gas Exploration and Development in Oklahoma." Oklahoma Geological Survey Special Publication 2000-2 (2000): 9-20.

PI Dwights Southern Midcontinent Well Production. PI Dwights. 23 Oct. 2008.

Rechlin, Kenneth J. "Reservoir Quality of the Frisco Formation, Hunton Group, Seminole County, Oklahoma (Part 1)." Shale Shaker (2005): 163-74.

Rechlin, Kenneth J. "Reservoir Quality of the Frisco Formation, Hunton Group, Seminole County, Oklahoma, (Part 2, Conclusion)." Shale Shaker (2005): 15-24.

Roehl, P. O. "Stony Mountain(Ordovician) and Interlake (Silurian) Facies Analogs of Recent Low-Energy Marine and Subaerial Carbonates, Bahamas:." AAPG Bulletin 51 (1967): 1979-2032.

Rottmann, Kurt. "Hunton Stratigraphy." Oklahoma Geological Survey Special Publication 2000-2 (2000): 21-38.

Swesnik, Robert M. "Geology of West Edmond Oil Field, Oklahoma, Logan, Canadian, and Kingfisher Counties, Oklahoma." AAPG Publication (1945): 359-98.

Taff, Joseph A. "Geology of the Atoka Quadrangle." U.S. Geologic Survey Folio 79 (1902).

VITA

Braydn Ross Johnson

Candidate for the Degree of

Master of Science

Thesis: PETROPHYSICAL STUDY OF THE WEST EDMOND FIELD IN PARTS OF OKLAHOMA, CANADIAN, KINGFISHER, AND LOGAN, COUNTIES, OKLAHOMA

Major Field: Geology

Biographical:

Personal Data: Born in Oklahoma City, Oklahoma, January 9, 1985, the son of Mr. and Mrs. Douglas W. Johnson. To be married to Melissa J. Dirik May 30, 2009.

Education: Graduated from Edmond Memorial High School, Edmond, Oklahoma, in May of 2003; received Bachelors of Science degree in Geology from Texas Christian University in August, 2007; completed requirements for the Masters of Science degree at Oklahoma State University in May, 2009.

Experience: Geological Intern, Chesapeake Energy, 2005-2008.

Professional Memberships: American Association of Petroleum Geologist; Society of Petroleum Engineers.

Name: Braydn Johnson Date of Degree: May, 2009

Institution: Oklahoma State University Location: Stillwater, Oklahoma

Title of Study: PETROPHYSICAL STUDY OF THE WEST EDMOND FIELD IN PARTS OF OKLAHOMA, CANDIAN, KINGFISHER, AND LOGAN, COUNTIES, OKLAHOMA

Pages in Study: 81 Candidate for the Degree of Master of Science

Major Field: Geology

Scope and Method of Study: The purpose of this study was to examine the Hunton Group reservoirs of the West Edmond Field in parts of Oklahoma, Canadian, Kingfisher and Logan Counties, Oklahoma. The objectives included: reconstructing the stratigraphy of the West Edmond Field using modern wire-line logs and recent advances in interpretations, establishing a depositional model and sequences for the upper part of the Hunton Group, examining previous reservoir engineering studies of the West Edmond Field to establish pathways of fluid migration and reservoir characteristics, and establishing dominant porosity types within the upper Hunton Group using whole core analysis, thin-sections, or scanning electron microscopy.

Findings and Conclusions: The Hunton Group carbonates include carbonate mounds (Frisco Formation), supratidal, intertidal, and subtidal carbonates deposited in a shallow ramp setting. Three petrophysical facies (A, B, and C) were identified that contain distinct lithologic characterisitics. Petrophysical facies A is composed of skeletal grainstones and packstones, facies B is composed of dolomitized skeletal wackestones, and facies C is composed of skeletal oolitic grainstones. Dominant porosity types include intraparticle pores in petrophysical facies A, intercrystalline pores in facies B, and oomoldic pores in facies C. Fracture porosity dominated fluid movement in early secondary recovery efforts. As a result recovery of oil and gas was highly inefficient. High fracture permeability and some interparticle pores in petrophysical facies A were depleted of oil and gas whereas lower-permeability zones if facies B and facies C contain economic reserves.

ADVISER'S APPROVAL: James Puckette